A Unipolar Pulse Electromagnetic Field Apparatus for Magnetic Therapy: design, simulation and development

Yuxiang Jiang

Thesis submitted to the
Faculty of Graduate and Postdoctoral Studies
In partial fulfillment of the requirements
For the M.A.SC. degree in
Electrical and Computer Engineering

School of Electrical Engineering and Computer Science
Faculty of Engineering
University of Ottawa
Ottawa, Canada

Abstract

As a magnetic therapy apparatus with medical benefits, the Unipolar Pulse Electromagnetic Field (UPEMF) apparatus is presented to produce unipolar pulsed magnetic waveforms with an intensity, shape, and frequency that meet medical requirements. The unipolar pulse is the most significant advantage, as the implemented apparatus is considered to be the first improvement in Pulse Electromagnetic Fields (PEMFs). The magnetic field is generated by a specially designed electromagnetic unit. In this unit, an electromagnet is concentrated by a designed concentrator to strengthen the magnetic field at the north pole and weaken the field on the opposite end. An electromagnetic shield is adopted to eliminate the effects of the south pole but allow the output from the north pole. Excited by a designed pulsed waveform generator, the electromagnetic unit generates a strong alternating-current magnetic field. In my work, the detailed design and development of the electromagnetic unit for UPEMF are introduced, therein being modeled and tested using Finite Element Method simulations. The model is characterized mathematically in three parts: the concentrator, the electromagnetic shield, and the overall unit. The testing and performance measurements of the actual Unipolar Pulse Electromagnetic Field apparatus are achieved using a Gauss meter and oscilloscope.

Acknowledgements

This research was funded by Houda Almansour Global Medical Devices & Design Inc, Canada.

I would like to express my sincerest appreciation to my supervisor, Prof. Abdulmotaleb El Saddik, for giving me the opportunity to conduct my research as well as for his guidance, support, patience and understanding for my whole graduate study period. His encouragement and valuable help made me persevere and finish my Master's research.

I would like to thank all the members of MCRLab for their help. I want to extend my appreciation of my colleague Dr. Haiwei Dong for his invaluable assistance and guidance during my research.

Finally, I would also like to thank my parents, who supported me unconditionally throughout my graduate studies.

Glossary of terms

- Two-dimensional (2D)
- Three-dimensional (3D)
- Pulsed Electromagnetic Field (PEMF)
- Uni-polar Pulsed Electromagnetic Field (UPEMF)
- Finite Element Method (FEM)
- Pulse Width Modulation (PWM)
- National Aeronautics and Space Adminstration (NASA)
- Transmembrane Potential (TMP)
- Photoplethysmograph (PPG)
- Electrocardiograph (ECG)
- Electroencephalograph (ECG)
- Tumor Necrosis Factor (TNF)
- Interleukins (ILs)
- Bipolar Junction Transistor (BJT)

Table of Contents

List of Figures

List of Tables

Chapter 1

Introduction

In this chapter, the background and motivation of the UPEMF apparatus are introduced. Then the objectives of the thesis are presented. The thesis is organized in the thesis outline.

1.1 Background and Motivation

The use of magnetic fields for therapy has a long history. Medical practitioners from China, Japan, ancient Greece, and Europe have successfully applied natural magnetic materials in their daily practice [34]. Many diseases, such as trauma and tissue damage,

are typically treated by surgery, and this invasive treatment is quite painful to many patients. In pursuing a non-surgical tissue restoration options, including muscle repair, non-union fractures and depression healing, the science of magnetic therapy has garnered enormous interest as an effective medical assistance method [43].

Magnetic therapy in general refers to the utilization of magnetic fields for effecting the charged particles in cells. A typical magnetic therapy is called pulsed electromagnetic field (PEMF) therapy. In the past two decades, the development of UPEMF devices has flourished, with huge demands and good application prospects.

Pulsed electromagnetic field (PEMF) therapy has been gaining importance since the space station was built in 1986 by NASA. After being in orbit around the earth for significant periods of time, the astronauts began to exhibit common symptoms of illnesses. These symptoms included muscle weakness, heart disease, osteoporosis, joint pain, and emotional disturbances such as depression and being socially withdrawn [18]. Medical doctors found that the reason for these symptoms was the reduction in the Earth's magnetic field due to the increasing distance from the Earth. Pulsed electromagnetic field (PEMF) therapy is regarded as an appropriate treatment for these symptoms [44]. NASA granted a patent [45] for PEMF. This patent used a simple coil to emit electromagnetic fields of a certain frequency and intensity to treat not only astronauts but also all elderly people who show the above symptoms. This treatment can be used as an assisting medical method and can even replace certain surgeries and medications [8].

PEMF cannot act on neutral structures but can act on individual structures such as the brain, muscles, and heart [26]. The following 4 tissues of individual structures are responsive to PEMFs:

- The electrically charged particles of the normal cells. The inner and outer membranes have different electrical gradients, called the transmembrane potential (TMP), due to the density of sodium and potassium. The inner membrane is charged to -70 mV. The exposure of the cells to PEMFs increases the negative potential of

the membrane from -70 mV to -90 mV. Consequently, the energy consumption is reduced during the pumping process of sodium and potassium.

- Stem cell activation. Exposure to PEMFs causes the TMP to be -90 mV, which acts as a shock wave to the stem cells leading to their activation [25].

- Collagenous protein conformation. The collagen is the main supportive protein of the human skeleton. PEMFs cause the same changes to the triple helix of the polypeptide chain's directions in the collagen.

- The transcription factor activation of the genetic material. PEMFs activate the transcription factors for neovascularization and the inhibition of tumor necrosis factor production (TNF) and interleukins (ILs) from the macrophages. Neovascularization is associated with the synthesis of new blood vessels, and thus, PEMFs are very effective in the treatment of coronary artery diseases, stroke, and peripheral ischemia because they open collateral blood vessels despite the main blood vessels narrowing.

Electromagnetic waves have three main parameters that make PEMFs of optimum medical benefit: (1) the frequency of the PEMF wave, (2) the shape of the PEMF wave, and (3) the intensity of the magnetic field. Differences in these parameters can lead to different therapeutic effects. Frequencies within a certain range and special types of shape waves with a certain scope of intensity can be used for medical therapies. These requirements are discussed in detail in the *Design Requirements*.

However, PEMF apparatuses currently on the market are varied. Their parameters are different, embodied by the intensity of the electromagnetic waves and the shape and frequency of the waveform. Thus, the medical effects of these devices have been questioned. The lack of industry standards of PEMF devices hinders the further development of research on magnetic therapy. To date, the known methods and devices that have been used for PEMF therapy, while generally suitable for their intended purpose, still have a

number of deficiencies from a variety of perspectives. For example, prior systems that utilize Helmholtz coils are less than ideal because such coils typically suffer from losses and field inhomogeneities.

Although PEMF apparatuses are abundant on the market and have various frequencies and intensities, they share certain main drawbacks: the magnetic field lines are curved and return back to the opposite pole quickly such that they cannot penetrate deeper tissue with maximum intensity to potentially heal the tissues. In other words, at the emitting end of the PEMF apparatus, the intensity of the magnetic field is not sufficiently strong due to the closed magnetic-field loop from the north end to the south end. Actually, the magnetic field suitable for our needs is the north end, which is the emitting end of the magnetic field lines. The most serious drawback of prior systems is that the generated field cannot penetrate deeply into the patient, and thus, the fields cannot be concentrated in certain remote lesions with sufficient energy for maximum effectiveness for a sufficiently short period of time. In addition, standards for the output waveform are not clearly defined.

The effects and inspection of electromagnetic medical treatments also require medical-related researchers to continue to conduct in-depth research. We thus perform our design and study based on the required magnetic field generator. The use of the instrument and its effects have yet to be verified.

The PEMF apparatus must be improved. In 2015, the patent *Uni-polar electromagnetic medical apparatus and methods of use* [19] proposed the first concept of unipolar PEMFs. This patent introduced the concepts needed to focus the magnetic field on one side and produce a unipolar magnetic field. The concept behind this device mitigates the drawbacks of current PEMF devices. The owner of this patent is Dr. Hossam, who is also the CTO of Houda Almansour Global Medical Devices. He proposed to combine the theoretical design of the patents with electromagnetic theory to build an actual prototype. In cooperation with Dr. Hossam, our research is based on his medical knowledge

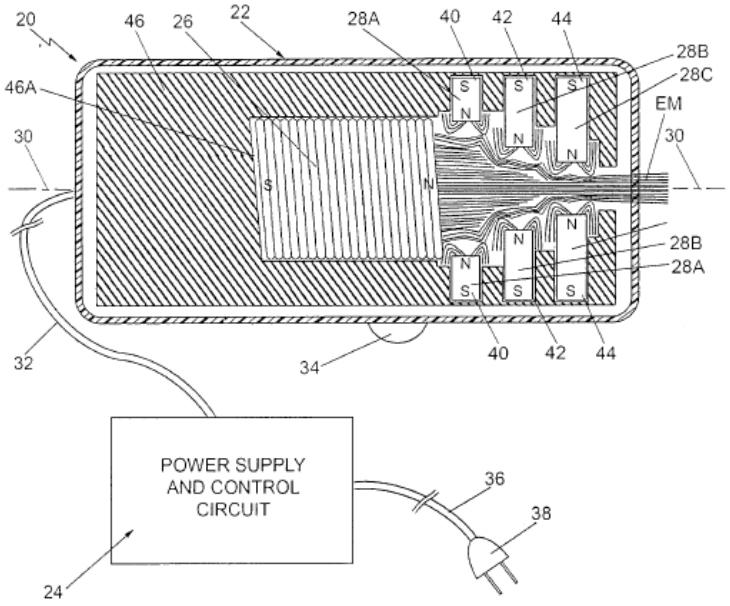

Figure 1.1: Sketch of UPEMF apparatus.

and research on UPEMF.

According to the patent in Figure 1.1, the key concepts of UPEMF are described as follows. The UPEMF device contains at least one pair of magnets for concentrated usage. The electromagnet, which is driven by a special power supply, is covered by a shell composed of Mu-metal. The wave of the electromagnet can only emit at the north pole.

Although this patent states the specific concept of the UPEMF apparatus, it did not provide detailed design and actual production information according to relevant physics knowledge. Since the owner of this patent focused more on the medical effects and less on the engineering design, this patent is not practical. We simulated the output waveform according to the patent. However, the output waveform did not meet our requirements. The drawbacks and limitations of the patent are described as follows:

1. The distance from the concentrated permanent magnets is too far from the magnetic core. Since the strength of the magnetic field decays with the distance cubed, the concentrator should be close to the northern surface; otherwise, the magnetic field will be too weak to provide medical effects. One way to solve this problem

is to increase the power of the electromagnet. However, the power required also increases exponentially. Moreover, the curve of the magnetic field line goes from the permanent magnet back to the south pole if the intensity of the magnetic field is sufficiently high. Under this circumstance, the permanent magnets have no concentration effects but rather play a role as the conductor.

2. The magnetic shield covering the north pole absorbs the output waveform. In this patent, the electromagnetic shield also covers the north pole, which means that the electromagnetic field will not be output from the north pole. The magnetic field line simply travels inside the electromagnetic unit, which means that no output or medical effects are obtained.

3. The magnetic shield should be close to the electromagnet. If the electromagnetic shield is too far away from the electromagnet, the magnetic field line will simply go from the north pole to the south pole inside the electromagnetic shield. This means that the output from the north pole is absorbed and thus cannot penetrate deeper tissue.

4. The detailed parameters of the desired electromagnetic wave should be defined as well. Although this patent mentions that the output waveform should be a pulsed wave, it does not define the shape, intensity, or frequency of the waveform.

5. The patent has yet to be developed into a prototype. This means that the detailed parameters of each part of the structure have yet to be determined.

Therefore, it is highly desirable to redesign and prototype this patent.

To improve the PEMF design, we need to redesign an improved pulsed electromagnetic field (PEMF) apparatus, called the unipolar pulsed electromagnetic field (UPEMF) apparatus [19]. Our presented instrument attempts to concentrate the electromagnetic field on the north pole of the apparatus, reduce the intensity of the south pole and satisfy

the parameter requirements for medical usage. By adding an electromagnetic field shield, the magnetic field line goes through the interior of the shield, which avoids emission at the south pole of the PEMF device. To strengthen the intensity of the north pole, a concentrator is applied around the electromagnet. For medical purposes, the power supply of the apparatus generates a positive square wave with an intensity of 1200 Gauss and a frequency of 30 Hz. The electromagnet part is carefully designed through Finite Element Method (FEM) simulations and driven by the power source.

1.2 Objectives

In our thesis, the whole process of the development of a unipolar pulse electromagnetic field apparatus for magnetic therapy is presented. We introduced and reviewed related technologies for UPEMFs. The design requirements are also discussed. The design and simulation processes are illustrated, and the first real-world UPEMF apparatus is developed.

The objectives of this thesis include the following:

- The UPEMF apparatus is redesigned to be practical to meet the requirements of magnetic therapy since there are drawbacks and limitations to the UPEMF patent. Each part of the new UPEMF apparatus is carefully designed and simulated.
- The design parameters of the UPEMF wave are clarified. Due to the different technical requirements of the products on the market, we have clearly defined the shape, intensity, and frequency parameters based on medical knowledge.
- A concentration method based on permanent magnets is presented. Inspired by the Halbach array, the concentration ring constructed by magnets is described mathematically. The concentration into a one-sided electromagnet is simulated and achieved.

- The FEM simulation of the UPEMF device is presented. The UPEMF physical model and differential form are described mathematically. Constitutive relations and boundary conditions are illustrated. The procedure and the important settings of the simulation are discussed in detail. The simulation results are visualized.

- The first UPEMF apparatus is developed. The chosen materials and production process are introduced. The testing and evaluation of the waveform are presented.

1.3 Thesis Outline

The thesis is organized as follows:

- Chapter 2 presents background and related work. Magnetic therapy and its medical effects are introduced. The popular pulsed electromagnetic field device and the drawbacks are analyzed. We summarize the numerical simulation method of the electromagnetic field and introduce the FEM.

- Chapter 3 describes the methodology and the design of our UPEMF apparatus in detail.

- Chapter 4 described the FEM model of our UPEMF mathematically. We present the detailed simulation process and results of our UPEMF apparatus. We visualize and analyze the simulation results.

- Chapter 5 provides the implementation details of the UPEMF apparatus and testing of the device.

- Chapter 6 concludes with the advantages and limitations of this research. Future work is also discussed.

1.4 Scholarly Output

Y. Jiang, H. Dong, H. Almansour, H. Mohamed, A. Saddik, "A Unipolar Pulse Electromagnetic Field Apparatus for Magnetic Therapy". *In: IEEE Instrumentation Measurement Magazine* (2018). (Accepted)

Chapter 2

Related Work

In this chapter, we introduce the related works of the UPEMF apparatus. Firstly, the pulsed electromagnetic field is introduced. We review the PEMF device. Some PEMF devices in the market are compared. We analyzed the limitations of the PEMF devices. Secondly, we present the concept of pulse power supply. Thirdly, the numerical simulation of the electromagnetic field is presented as the simulation method.

2.1 Pulsed Electromagnetic Field

An electromagnet is a device that generates a magnetic field after the energization of a multi-turn coil. It can convert electrical energy into magnetic energy and then use the generated magnetic field to convert the magnetic energy into other forms of energy. The electromagnet is mainly composed of a multi-turn coil and a core. Iron cores are generally made of soft magnetic materials. The coil is achieved by winding a copper wire of a certain diameter around a stationary coil support.

There are many types of electromagnets. According to their applications, the main types of electromagnets are as follows: (1) electromagnetic relays, (2) lifting electromagnets, and (3) electromagnetic vibrators. According to their current sources, the main types of electromagnets are as follows: (1) DC electromagnets, where the magnetic flux created by this DC excitation is a constant magnetic flux, i.e., it does not change with time, and (2) AC electromagnets, where the magnetic flux density changes with the frequency of the power supply, and thus, hysteresis and eddy current losses occur in the electromagnet.

Pulsed magnetic fields are a type of periodic AC magnetic field. Unlike ordinary static and AC magnetic fields, pulsed magnetic fields are intermittent and periodic. The peak and trough are quite different. However, the ratio of the time from the crest to the trough and the rising edge of the trough to the crest represents a small proportion of the period of the waveform. In intermittent pulse generation with intermittent pulse currents, the current flow through the solenoid coil can produce a variety of shapes of the pulsed magnetic field. The pulsed magnetic field is characterized by intermittent magnetic fields, changes in the frequency of the magnetic field, and waveforms and peaks can be adjusted as needed.

PEMFs, electromagnetic fields used for medical research, have been extensively studied. M. J. Stiller [34] provided an assessment on the healing of recalcitrant venous ulcers

by a portable pulsed electromagnetic field (PEMF). The result of his study indicated that PEMF stimulation effectively and safely enhances the healing of recalcitrant venous stasis ulcers. Pericles Diniz [37] presented the effects of PEMFs with 15 Hz pulse bursts with a 7 mT peak. PEMF stimulations of bone tissue-like formation on osteoblasts in different stages of maturation were assessed to determine whether the PEMF stimulatory effect on bone tissue-like formation was associated with an increase in the number of cells and/or with the enhancement of cellular differentiation. Dean Cvetkovic [9] conducted an experimental pilot study to investigate the effects of PEMFs at extremely low frequency in response to human signals, including photoplethysmographs (PPG), electrocardiographs (ECG), and electroencephalographs (EEG). The evidence shows that PEMFs affect human tissues and cells.

The production of PEMF devices has increased significantly. L. R. Tejera described his design and development of a PEMF device in his thesis [29]. He performed the project through four subsystems perfectly coupled together: a waveform generator, an amplifier, two electromagnetic coils and a digital voltmeter. The waveform from the generator is amplified by the amplifier and detected by the sensor coil. The final output of the magnetic field has a peak of 15 mT at a frequency of 100 Hz. A PEMF generator was designed by M. R. Bayatiani [35] with Helmholtz coils that can produce nearly uniform magnetic fields with different frequencies from 0 Hz to 300 Hz and intensities from 0 mT to 8 mT. A quantum resonance system [38] built by P. Liwluck is a type of PEMF device. He used this system to test the effects on brainwaves.

The parameters for some PEMF devices on the market are shown in Table 2.1. The Sota MP6 has a strong magnetic field, capable of 0.6 T, but the field is bipolar, and the frequency is low. This type of PEMF instrument requires a long time to store the energy and then instantaneously releases this energy to generate the pulse. Thus, the frequency cannot be high because of the low power. The OMI and iMRS are devices with low pulse strengths but high-frequency outputs. The strength of the field is less than 100 μT, but

Figure 2.1: PEMF devices on the market. The instruments from left to right are Sota MP6, OMI, and iMRS.

Table 2.1: Parameters of PEMF device in the market

Product name	parameters (strength, direction, frequency)
Sota MP6	0.6 T, Bipolar, 0.19 Hz
OMI	66 μT, Bipolar, 30 Hz
iMRS	70 μT, Bipolar, 30 Hz

the frequency can be greater than 30 Hz. Due to the low strength, the process of storing power is quick.

A wide variety of PEMF instruments have different parameters. The intensity of the pulse is different, being on the order of micro Tesla to high field strengths, and the frequency varies from 0 Hz to 1000 Hz. There is no single standard on the market to show which type of product or which parameters are more beneficial to medical care. Therefore, it is very important and necessary to combine the specifics of these products and refer to relevant medical research to determine the parameters of the PEMF in constructing an instrument capable of best achieving the medical effects of PEMFs.

2.2 Pulse Power supply

As a fundamental aspect of variable electrical equipment, power supplies provide power shaping and delivery [21]. Power supplies are used to implement power shaping and power transfer. They have been widely applied to various fields such as industrial production,

energy, transportation, information technology, and aerospace.

In the power industry, there are several types of power supplies, including switching power supplies [17], linear regulator power supplies, electrolysis power supplies, sine wave power supplies, AC variable frequency power supplies, and high-power high-voltage DC power supplies.

The PEMF waveform is generated by an electromagnet that needs to be driven by a special excitation source, which is a pulse power supply, to generate the required waveform from the electromagnet. Our pulse power is also a special type of switching power supply. As its name suggests, its voltage and current waveforms are pulse-like, being determined by the output characteristics of the pulsed power supply, and have different classifications such as high frequency, low frequency, unipolar, bipolar, high voltage, and low voltage, and specifically selects the type of output voltage, output current and switching frequency depending on the given application. In addition, the power supply produces rectangular, triangular, saw-tooth, cosine and other waveforms.

The power supply needs to be charged intermittently, that is, for a certain time period, the power supply is charged, and then, the power is turned off for a certain period of time. This repeating charging and discharging constitutes a pulsed power supply. After a sufficiently slow energy storage process, the primary energy source achieves sufficient energy. Then, the intermediate energy storage and pulse shaping system are charged (inflow energy), and the energy is ultimately discharged after some complicated processes, such as storage, compression, pulse formation and conversion, are performed.

The performance of a pulsed power supply largely depends on the development of switching devices, especially high-power pulsed power supplies [3]. Switching device stacks play an important role in improving circuit performance, reducing circuit losses, and improving current use efficiency. With the development of power elements, such as the standardization and integration of switching elements, such as power MOSFET, insulated-gate bipolar transistors (IGBTs), and gate turn-off thyristors (GTOs), the per-

formance of various aspects of pulsed power supplies has been significantly improved.

2.3 Numerical Simulation of the Electromagnetic Field

Since Maxwell developed the classical theory of electromagnetic fields in 1865, electromagnetic field technology has not only demonstrated its important role in the field of strong and weak electrical engineering, with the transmission and transformation of electromagnetic energy and information as the core, but also has been involved in military, geological, ecology, medical and many other fields, therein being combined with a variety of technologies and facilitating the development of many new technologies [4].

Based on the complexity of engineering electromagnetic fields, the complexity of various electromagnetic devices in terms of their structure and geometry, as well as the complexity of material property changes (the material permeability, conductivity and specific heat capacity and other parameters vary with temperature), results in problems in a variety of analytical methods used in electromagnetic field analysis and calculation such as separation of variables, conformal transformation, the mirror method and the Green's function method [47]. These methods cannot adapt to the needs of a wide range of engineering problem analyses. With the rapid development of computing technologies over the years, numerical calculation methods for electromagnetic fields in the category of approximate calculation methods have been widely developed and can finally meet the actual requirements of the precise analysis of mathematical models in science and engineering.

The basic aspects of electromagnetic fields in various electromagnetic devices belonging to the field of electromagnetic field analysis are common. Given a certain calculation area, the compositions and characteristics of the materials in each area, and the characteristics of excitation sources, the field quantities and the space-time distributions of the fields are calculated. This is the computation problem for electromagnetic fields.

Therefore, the calculation of electromagnetic fields corresponding to electromagnetic field numerical analysis is based on the basic governing laws of electromagnetic fields, i.e., Maxwell's equations. First, a continuous mathematical model approaching the problem of electromagnetic fields in practical engineering is established. Second, using the corresponding numerical calculation method, through discrete processing, the continuous mathematical models are transformed into equivalent discrete mathematical models, which are discrete algebraic equations of discrete numerical systems. Third, using the effective algebraic solution, the discrete solution of the discrete mathematical model, i.e., the numerical solution of the field values, is calculated. Finally, based on the discretization of the field quantities (including the bit functions) of the obtained electromagnetic field problem and the various post-processing processes, the field strength at any point in the desired field, such as the energy of any region, consumption distribution, force, torque and various types of electromagnetic parameters and performance indicators, can be obtained. After applying these processes, we can analyze the electromagnetic problem in engineering theoretically, make engineering decisions based on the results and optimize the given design.

Chapter 3

Unipolar Pulsed Electromagnetic Field Apparatus

In this chapter, based on the motivation of the UPEMF system, we introduce the details of the design requirements, i.e., the three most-significant parameters that the generated electromagnetic waveform should satisfy. To meet these parameters, we developed the overall structure of the UPEMF system and presented the design methods and design details. Based on the design of the electromagnetic unit, the corresponding excitation source design method is presented.

3.1 Design Requirements

There are three main parameters, i.e., the frequency, shape and intensity, that can be used to make the UPEMF of optimum medical benefit, as introduced in Chapter 2.

3.1.1 Frequency of the UPEMF Wave

Lower frequencies, such as that of the Earth (8 to 11 Hz), are essential for normal and healthy tissue. Sick or degenerative tissue must be treated with higher frequencies than those of the Earth's magnetic field. Each tissue has a frequency threshold whereby it starts to resonate at or above this threshold. We cannot stress enough that the threshold means the minimum frequency below which the tissue cannot resonate but whereby it can resonate above it. For example, bone resonates at 24 Hz and is considered the tissue that requires the highest frequency to resonate. Therefore, for all tissue of the body to resonate, the frequency has to be greater than 24 Hz [36]. This frequency is higher than the thresholds (24 Hz) of all tissue of the human body.

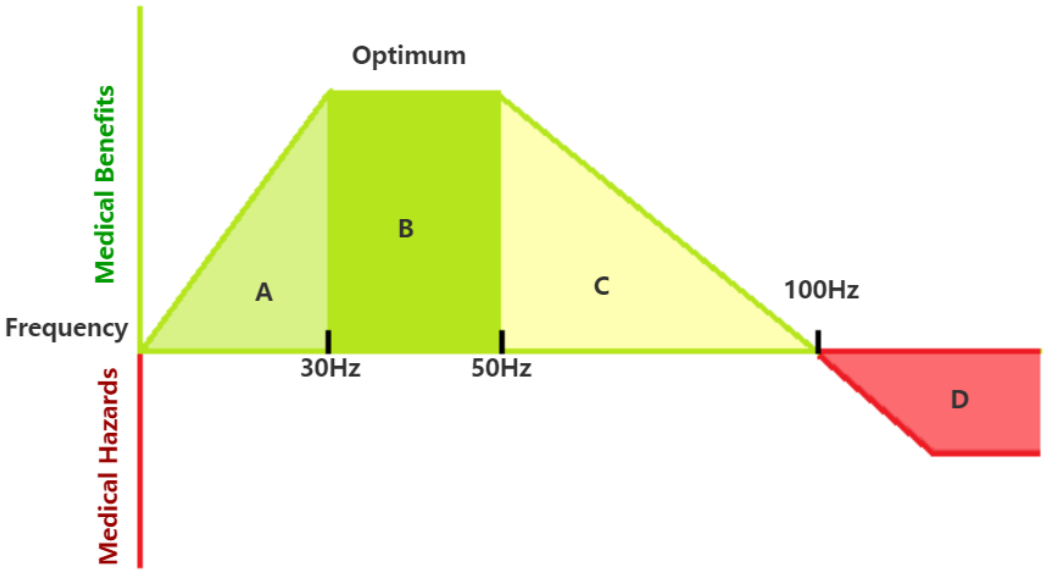

Figure 3.1: Optimal frequency of medical benefits.

The Earth's magnetic field frequency is equal to the alpha waves of the brain: 8-11

Hz. Research has shown that increasing the frequency leads to a better result up to 30 Hz [32][36]. The frequency range with medical effects is shown in Figure 3.1. From 30-50 Hz (region B), the medical benefits present a plateau. From 50 to 100 Hz (region C), the medical benefits gradually decrease. Above 100 Hz (region D) is not recommended because high frequency of wave causes harm to the body. The medical benefits become minimal or go away completely [32]. Therefore, we chose an optimum frequency within region B: 30 Hz.

3.1.2 Shape of the UPEMF Wave

Our desired pulse waveform is a type of time-domain periodic signal with repetitive changes in instantaneous amplitude over time. The general expression of a periodic signal is as follows:

$$X(t) = X(t + kT), k = 1, 2, 3... \tag{3.1}$$

where t is the time and T is the period.

There are three typical pulse waveforms for PEMF: (a) sine waves, (b) triangle waves, and (c) rectangular waves. The mathematical expressions used to describe these waveforms are as follows:

$$X_s(t) = Asin(\omega t + \varphi) + b$$

$$X_t(t) = \begin{cases} 0,\ 0 < t < t_1 \\ \text{At+b},\ t_1 < t < t_2 \\ \text{-At+b},\ t_2 < t < t \end{cases}$$

$$X_r(t) = \begin{cases} \text{A},\ 0 < t < t_1 \\ 0,\ t_1 < t < T \end{cases}$$

where A is the amplitude, ω is the angular frequency, φ is phase, b is bias.

The medical benefits are variable according to the shape of the wave. A sine wave

(Figure 3.2 (a)) has no or very limited medical effects. A saw teeth wave (Figure 3.2 (b)) could have moderate medical benefits.

The best medical benefits can be obtained by the rectangular wave (Figure 3.2 (c)). The cell membrane which is formed of double layers phospholipid act as an electrically and osmotically isolating material [26]. The cell membrane has minute channels that called transmembrane channels. These channels can allow passage of ions mainly sodium and potassium. The main action of PEMF is abrupt rise and fall of the magnetic field which can create the transmembrane potential of the cell membrane. Slow raising and fall of the magnetic field as in case of sine wave allows the transmembrane channels to compensate for the change of magnetic field by allowing the ions to pass through these channels. The transmembrane potential exhibits either minimal electrical changes or

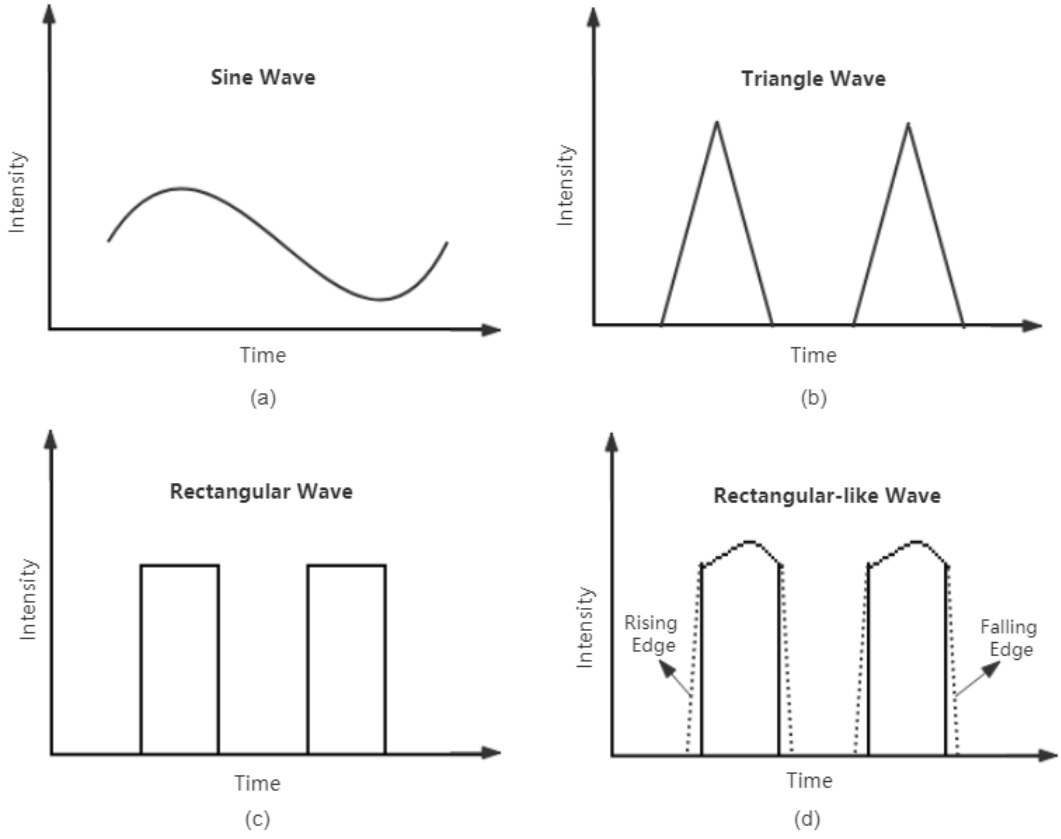

Figure 3.2: Optimal frequency for medical benefits.

even no changes at all. This is because a time is given for the channel to compensate by

allowing ions to pass through them. In the case of a rectangular wave, no time is allowed for the channels to compensate. Thus, the change in the magnetic field is associated with an electrical current through the transmembrane potential. Compared to the triangle wave, the rectangular wave has a platform at the peak value which maintain a short time. That means the affect to transmembrane transmission is better. In conclusion, a UPEMF wave with better medical benefits has a waveform with steep rising and steep falling edges. Meanwhile, the wave should remain at the desired intensity for some time before it decreases in intensity. In actual use, an ideal rectangular wave with a smooth peak cannot be achieved. The sudden change in an ideal rectangular wave is an instantaneous transition. In actual circuits, the pulse voltage changes from zero to the maximum value and from the maximum value to zero in a non-zero amount of time, causing a rising edge and falling edge, respectively. As a result, the goal in generating a proper pulsed electromagnetic waveform shape is to create rectangular-like waveforms (Figure 3.2 (d)). The rectangular-like waveforms have fluctuations at the peak as well as rising and falling edges.

3.1.3 Intensity of the UPEMF Wave

NASA studies have shown that there is a biological window in which tissue can resonate maximally [44]. The biological window of Adey is such that the intensity at the affected site should be close to 10, 200, or 500 Gauss with regard to the inverse square law (ISL) [31]. This law means that the intensity is reduced proportional to the second power of the distance between the emitting solenoid and the diseased-affected site. For example, if the diseased site is in the heart and it is away from the skin by 7 cm, the intensity is reduced by 49 times that from the emitting solenoid provided that the solenoid is attached to the skin. Based on the above situation and practical concerns, we adopted 0.12 T (1200 Gauss) as the maximum intensity of the UPEMF wave.

3.2 Overall System

The proposed unipolar electromagnetic field system is essentially a pulsed magnetic generator. The system consists of two parts. The first part is the electromagnetic unit, which is driven by a time-varying source carrying the driven alternating current (AC). The second part is the pulsed power source, which generates the input current with a certain waveform shape and frequency. The first part is driven by the second part and emits the medical-use waveform.

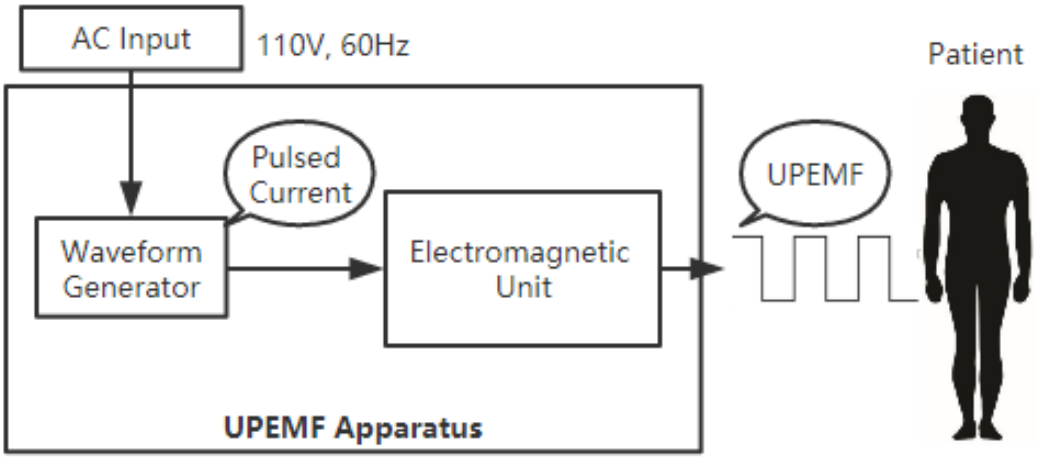

Figure 3.3: Unipolar Pulsed Electromagnetic Field System.

The application architecture of the proposed UPEMF system (Fig. 1) has two main parts, where the electromagnetic unit is the main design target:

- The electromagnetic unit, which produces the required UPEMF wave. The output waveform is a rectangular wave with an optimized frequency of 30 Hz and intensity of 0.12 T.

- The waveform generator, which is used for producing the desired input of the electromagnetic unit. The pulse must be high enough to offset the induction voltage.

3.3 Electromagnetic Unit

The design consists of three parts. The first part is the magnetic core (made using silicon lamination) and the multi-turn coils (made of copper), which generate the magnetic field according to the number of turns and the current. The second part is the concentrator. The concentrator consists of pairs of permanent magnets constituting a magnet ring. The concentrator increases the strength of the field near the central axis of the cylinder. The third part is the magnetic shield. The shield absorbs the magnetic field; thus, we only use it to eliminate the effects of the south pole and avoid field interactions.

3.3.1 Magnetic Core

The magnetic core is usually composed of materials with high permeability (μ). The magnetic field is created by a current-carrying coil of wire around the magnetic core [15]. A magnetic core is used to confine and guide the electromagnetic field. Thus, the magnetic field lines are concentrated along the magnetic core. The most popular magnetic cores are composed of iron or ferrite. These materials can be easily magnetized by the magnetic field from the coils.

However, after removing the external magnetic field following magnetization to saturation, these types of magnetic cores can still maintain a certain magnetization in the original direction [33]. This phenomenon is called remanence ($\mathbf{M}_r$). It does not cause problems if we only consider magnetostatics. However, in our case of UPEMF waves, the electromagnetic wave is fluctuating following certain requirements. The remanence has significant effects on the shape and strength of the field, causing distortions of the waveform. To demagnetize the electromagnet immediately, we produce a magnetic core using a silicon steel sheet to achieve faster demagnetization.

The process of magnetization is described by the hysteresis loop [11] in Figure 3.4 (a). Starting from the residual magnetization $\mathbf{M} = 0$, the magnetic field strength $\mathbf{H}$ of the

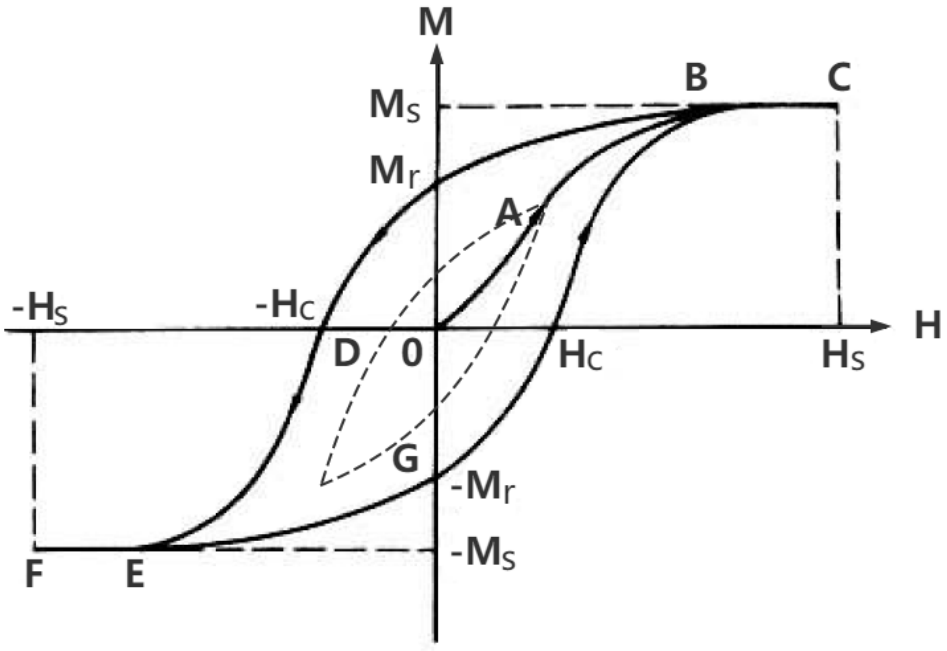

Figure 3.4: Magnetization curve is explained as hysteresis loop.

magnetization field is gradually increased, and the magnetization M increases along the OABC curve until it reaches the magnetization saturation state **B**. The OABC curve is called the initial magnetization curve. $\mathbf{M}_s$ is the saturation magnetic flux density. When reducing the magnetization field, the magnetization curve from point B does not return along the initial magnetization curve. When H is reduced to zero, $\mathbf{M} \neq 0$ but rather is equal to the residual magnetization $\mathbf{M}_r$. To reduce **M** to zero, a reverse magnetization field must be applied. When the reverse magnetization field is strengthened to $-\mathbf{H}_c$, $\mathbf{M} = 0$. $\mathbf{H}_c$ is called the coercivity. This phenomenon indicates that the change in magnetization M lags behind the change in H, which is called hysteresis.

$$\mathbf{B} = \mu(\mathbf{H} + \mathbf{M}) \tag{3.2}$$

The CBDEF curve describes the demagnetization process until reverse saturation. Corresponding to the CBDEF curve, FEGBC describes the magnetization process from reverse to positive saturation. If there is no saturation, the hysteresis loop will follow the dotted

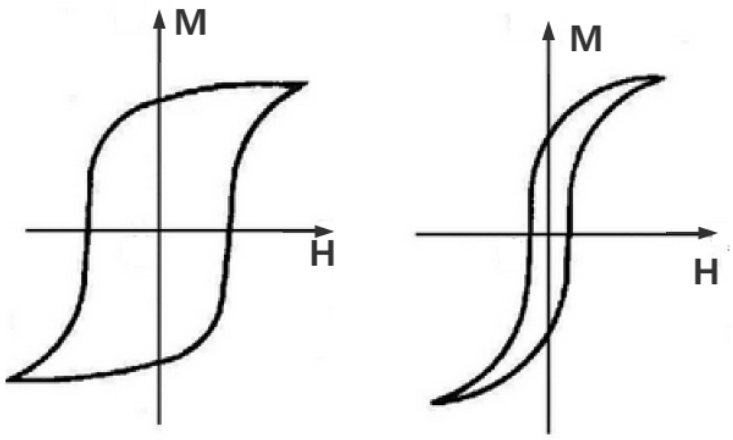

(a) Hysteresis loop of non-soft magnetic materials.

(b) Hysteresis loop of soft magnetic materials.

Figure 3.5: Explanation and comparison of hysteresis loop.

line.

The magnetization of magnetic materials in repeated positive and reverse magnetic fields will produce heat. The generation of this heat is via the applied magnetic field. The power loss is directly proportional to the size of the area enclosed by the hysteresis loop.

Compared to regular magnetic materials, silicon steel has a narrow hysteresis loop since it is a type of soft magnetic material. Its demagnetization is fast, and the remanence is low. As a result, power losses are minimal.

In addition to a narrow hysteresis loop, the performance of a silicon steel sheet is better than silicon steel alone [16]. A silicon steel sheet is made by rolling several silicon steel pieces. The gap between each silicon steel piece is achieved using an insulating material. Therefore, the electric resistance of a silicon steel sheet is very high. The loss caused by eddy currents decreases [27].

In conclusion, our magnetic core adopted a silicon steel sheet as the material for the following three reasons:

- The hysteresis losses are low because of the narrow hysteresis loop.

- The eddy current losses are low because of the high electric resistance.
- The strength of the magnetic induction is high in a strong magnetic field. This reduces the core size and weight, reducing the copper wire requirements.

The geometry of the designed magnetic core is a cuboid. The silicon steel production process is very complicated. A custom-made cylindrical silicon steel sheet would be too expensive. Although the performance of a cylinder is better, we still used a cuboid.

3.3.2 Concentrator

Since our UPEMF is a one-sided magnetic field, the concentration of the magnetic field at the north pole but not at the south pole is needed. Although increasing the input current density and the number of turns of the coil are two ways to strengthen the magnetic field, they increase the intensities at both the south and north poles. The concentration of the field at the north pole is important. The limitation presented by the power supply restricts the design. Moreover, a smaller electromagnet is desired so that the UPEMF apparatus can be easily transported. Considering the augmentation of the north pole and for increasing the energy efficiency, a special concentrator should be utilized that attempts to increase the magnetic field at the north pole using a ring permanent magnet.

The scheme is inspired by the Halbach array [23] and adopts the design of the concentrator used in magnetic rendering systems for haptic displays [41]. A Halbach array is a special arrangement of permanent magnets that augments the magnetic field on one side of the array while canceling the field to near zero on the other side [39]. A typical 2D Halbach array has an arrangement as shown in Figure 3.6. Each block is a permanent magnet. The arrows in the block represent the magnetization of the magnet. The arrows in Figure 3.7 indicate the direction of the magnetic field. As shown in Figure 3.7, the magnetic field is augmented on the top side and reduced on the bottom side.

Symmetrically, at least one pair of magnets on the right side of the north pole is

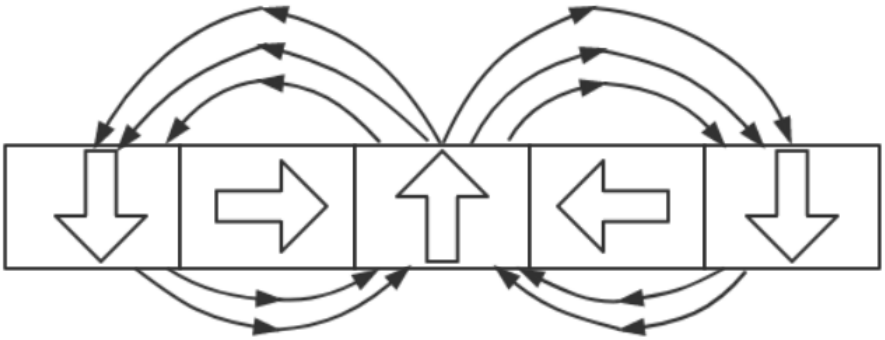

Figure 3.6: Arrangement of a 2D Halbach array.

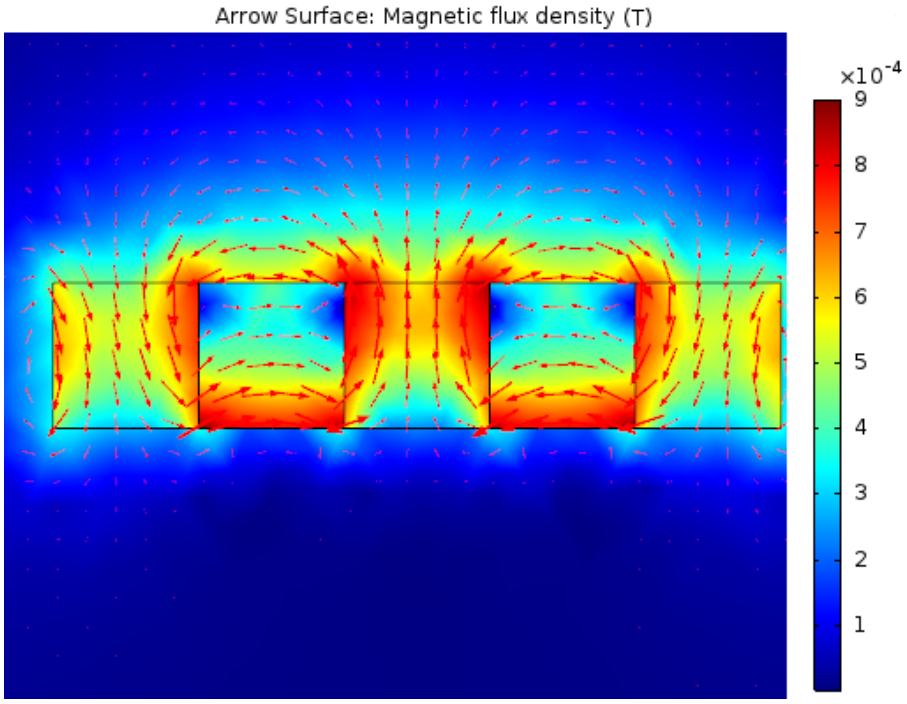

Figure 3.7: Magnetic field of a 2D Halbach array in simulation.

applied. The combination of numerous pairs of small magnets is the concentration ring. Since the reduction in the strength of the magnetic field goes as the distance cubed, the strength of the field decreases significantly with increasing distance from the north pole surface. Thus, the concentrator should not be excessively strong at the north end of the electromagnetic unit.

In Figure 3.8, we consider the top as the north pole of the electromagnetic unit and the bottom as the south pole. The cylinder ring is uniformly radially magnetized with a direction from the outer to inner ring, which points to the center of the circle. The concentrating permanent magnet ring contributes to the top surface current with a counter-clockwise magnetization current and to the bottom surface current with a clockwise magnetization current. When calculating the magnetic field, the surface current on the top and bottom can be replaced in the calculation of the volume magnetization. $\mathbf{M}(\vec{r}, \vec{\phi}, \vec{z})$ is used to express the magnetization vector field in the cylindrical coordinate system. $\vec{r}, \vec{\phi}, \vec{z}$ is cylindrical coordinate system in Figure 3.8. The magnetic field in cylindrical coordinates can be written as

$$\mathbf{M}(\vec{r}, \vec{\phi}, \vec{z}) = M_r(\vec{r}, \vec{\phi}, \vec{z})\vec{r} + M_z(\vec{r}, \vec{\phi}, \vec{z})\vec{z} + M_\phi(\vec{r}, \vec{\phi}, \vec{z})\vec{\phi} \tag{3.3}$$

where M_r, M_z, and M_ϕ are the magnitude of each component of the magnetic field. In our design, the magnetization direction is along $-\vec{r}$ and has magnitude M_r, which is written as

$$\mathbf{M}(\vec{r}, \vec{\phi}, \vec{z}) = -M_r\vec{r} \tag{3.4}$$

$\nabla \times \mathbf{M}(\vec{r}, \vec{\phi}, \vec{z})$ is the curl of the vector field, which can be written explicitly as

$$\nabla \times \mathbf{M}(\vec{r}, \vec{\phi}, \vec{z}) = (\frac{1}{r}\frac{\partial M_z}{\partial \phi} - \frac{\partial M_\phi}{\partial z})\vec{r} + (\frac{\partial M_r}{\partial z} - \frac{\partial M_z}{\partial r})\vec{\phi} + \frac{1}{r}(\frac{\partial (rM_\phi)}{\partial r} - \frac{\partial M_r}{\partial \phi})\vec{z} \tag{3.5}$$

The magnetization current densities for a cylinder ring are then calculated by

$$\begin{aligned} \mathbf{J}_{VM} &= \nabla \times \mathbf{M}(\vec{r}, \vec{\phi}, \vec{z}) \\ &= \nabla \times (-M_r)\vec{r} \\ &= \vec{0}(A/m^2) \end{aligned} \tag{3.6}$$

where $\mathbf{J}_{VM}$ is the volume magnetization current density. The simplified output of the calculation for a cylinder ring is $(-M_r)\vec{r}$, where M_r is a positive constant representing the magnitude of the magnetization. The equivalent surface magnetization current densities are calculated as follows:

$$\begin{aligned} \mathbf{J}_{SM}^{top} &= \mathbf{M}(\vec{r}, \vec{\phi}, \vec{z}) \times \vec{n} \\ &= (-M_r)\vec{r} \times \vec{z} \\ &= M_r\vec{\phi}(A/m^2) \end{aligned} \tag{3.7}$$

$$\begin{aligned} \mathbf{J}_{SM}^{bottom} &= (-M_r)\vec{r} \times -\vec{z} \\ &= -M_r\vec{\phi}(A/m^2) \end{aligned} \tag{3.8}$$

$$\begin{aligned} \mathbf{J}_{SM}^{inner} &= (-M_r)\vec{r} \times -\vec{r} \\ &= \vec{0}(A/m^2) \end{aligned} \tag{3.9}$$

$$\begin{aligned} \mathbf{J}_{SM}^{outer} &= (-M_r)\vec{r} \times \vec{r} \\ &= \vec{0}(A/m^2) \end{aligned} \tag{3.10}$$

where $\mathbf{J}_{SM}^{top}$, $\mathbf{J}_{SM}^{bottom}$, $\mathbf{J}_{SM}^{inner}$, and $\mathbf{J}_{SM}^{outer}$ are the surface magnetization current density on the top, bottom, inner, and outer side, respectively.

From Equation 3.6 to Equation 3.9, the concentrator only contributes the top and bottom surface currents, which have are in opposite directions. On the top surface, the counter-clockwise magnetization current is in the same direction as the stimulating current. According to Ampère's right-hand rule, the current on the top surface generates a north pole magnetic field; thus, the field on the north pole is increased. Similarly, the clockwise magnetization current on the bottom surface has the opposite direction to the stimulating current. Therefore, the field on the south pole is reduced.

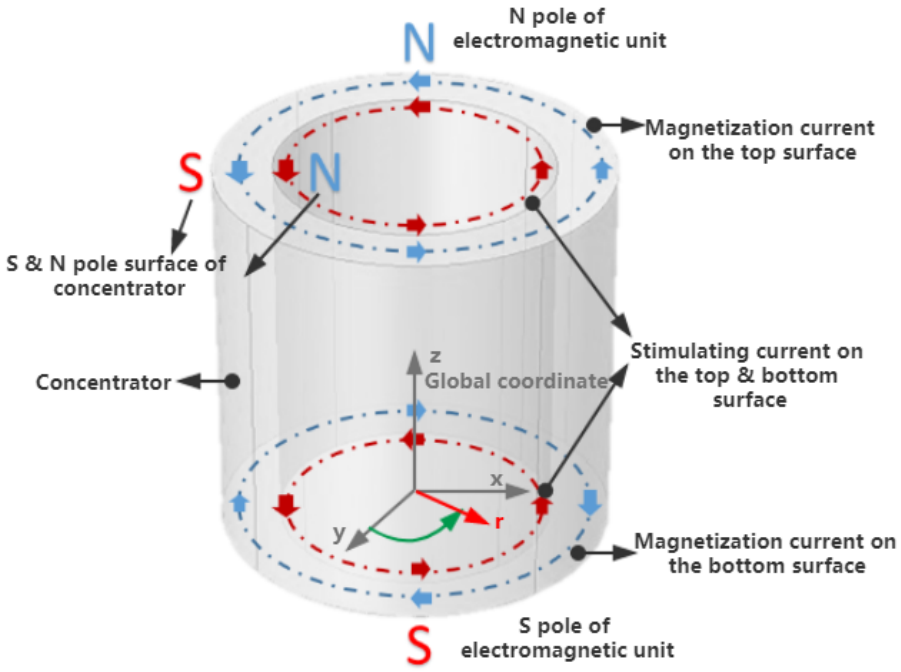

Figure 3.8: Mechanism of magnetic field concentrator in the global coordinate system as a function of magnetization current.

After simulation, the magnetic field distribution (Figure 3.9) shows that the transmission ends of the north pole are the top and bottom. The size of the yellow arrows expresses the strength of the magnetic field. The magnetization of the top surface is in the same direction as the coils stimulated by the current, whereas the bottom surface is the opposite. Thus, the UPEMF is enhanced at the north pole and reduced at the bottom surface when the concentrator is added. The magnetic field from the south pole is reduced to achieve unipolar magnetization.

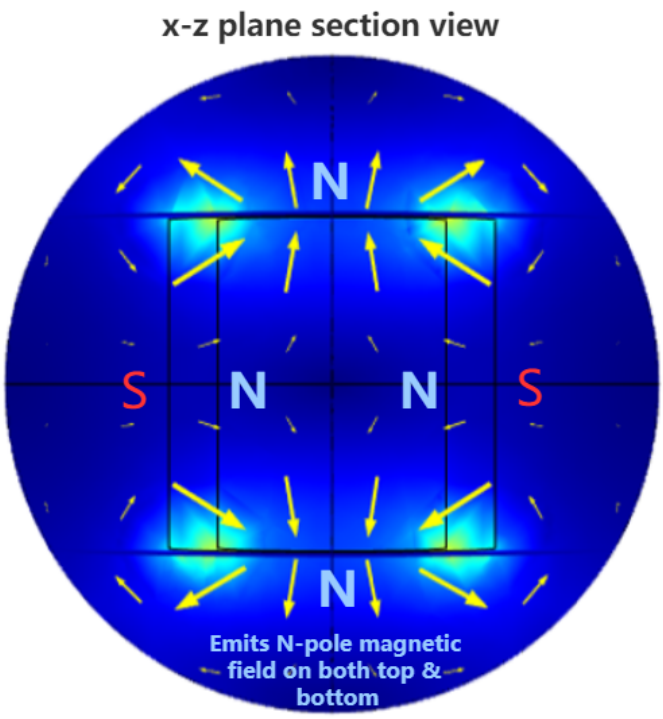

Figure 3.9: Visualize the magnetization and the resulting magnetic direction.

3.3.3 Magnetic Shield

The electromagnetic shield [42] is used to isolate the magnetic field from the electromagnet, which only allows the field to emit from the north pole. Shielding is metal isolation between two spatial areas used to control the induction and radiation of magnetic and electromagnetic waves from one area to another. The magnetic shield has several main features

- When the required electromagnetic field frequency to be shielded against is high, we use low-resistance metal material generating an eddy current, the formation of electromagnetic wave counteraction, to achieve the shielding effect.

- When the frequency of the electromagnetic wave to be shielded is low, a material with a high magnetic permeability is used so that the magnetic induction line is confined to within the shielding body to prevent diffusion to the outside of the

shielding space.

- In some cases, we often use different metal materials to construct a multi-layer shield if we require good shielding for high-frequency and low-frequency electromagnetic fields.

For low-frequency magnetic fields, including magnetostatics, when the frequency of the magnetic field is lower than 100 kHz, the shielding measures depend mainly on the magnetic shunting effect of the magnetically permeable material. In this case, the eddy current shield effect is small.

Materials with high permeability are suitable for shielding. High-permeability materials can be considered as a channel with lower reluctance compared to air. Most of the magnetic field is absorbed by the material, and the magnetic field of the electromagnet forms a closed loop via the shield. Thus, the electromagnetic shield can shield the radial magnetic field and the south pole of the electromagnet.

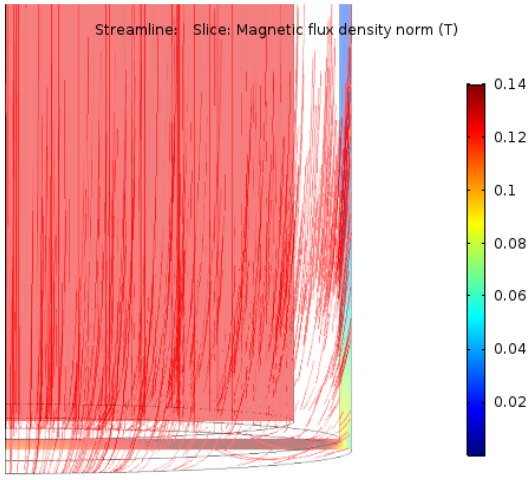

Figure 3.10: Magnetic field shielding.

One typical material used in magnetic shielding is Mu-metal. Mu-metal is a nickel-iron soft magnetic alloy with very high permeability and is used for shielding static and low-frequency magnetic fields. Mu-metal typically has a relative permeability of 80,000–100,000, compared to several thousands for ordinary steel.

The cross section of the length of the electromagnetic is shown in Figure 3.10. the red lines indicate the induction lines. There are no lines in the outer area (air). The lines spreading to the outer area are retained in the Mu-metal shell. The shape of the magnetic shield is a half-open cylindrical chamber closed only at the south end, while the north pole is exposed.

3.4 Excitation Source

It is very important to design a power source that can excite the electromagnet. The design of the pulsed power supply determines whether our electromagnet can produce the required waveform. In this section, we first make a rough estimate of the parameters required to generate the magnetic field, and then, we use this estimate to design the magnetic field power supply. In Chapter 4, we will discuss the detailed design and simulation of the electromagnets based on the estimation.

3.4.1 Magnetic Field Estimation

Before designing the power supply and conducting the electromagnet simulation, we need to perform a rough calculation of the parameters of the electromagnetic that generates the magnetic field so that we can use this as a reference for subsequent design and simulation.

Our electromagnet is a finite-length energized solenoid consisting of a multi-turn coil [2]. The multi-turn coil can be considered as being formed by the superposition of N energized rings [40]. We first study the magnetic field distribution of a single energized ring.

The ring model is shown in Figure 3.11. The ring current with a radius R and magnitude I is in the *xoy* plane, and the center of the circle is the origin of the coordinates. According to symmetry, only the magnetic field in the *xoz* plane is required to determine

the magnetic field distribution in the entire space.

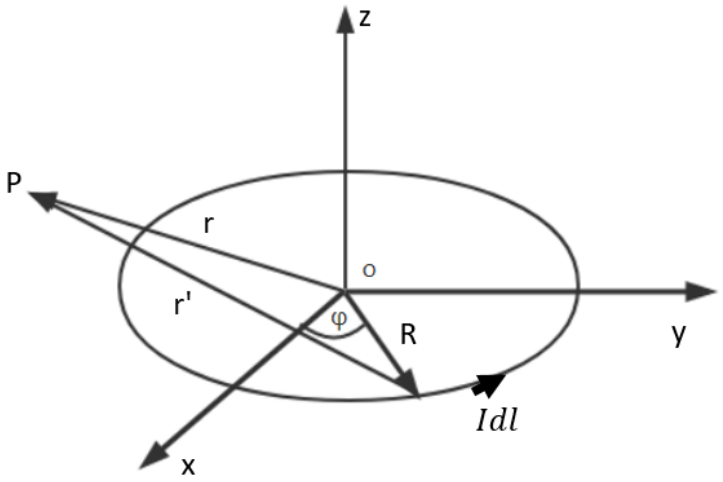

Figure 3.11: Magnetic ring model.

Let P be in the xoz plane shown in Figure 3.11, and we use Cartesian coordinates (x, y, z) and cylindrical coordinates (ρ, φ, z). The relationships between these coordinate systems are

$$x = \rho cos\varphi$$

$$y = \rho sin\varphi$$

$$\rho = \sqrt{x^2 + y^2}$$

It can be seen from the diagram that the coordinates of P are $(\rho, 0, z)$, and Q is a point on the circumference of the circle current; its coordinates are $(R, \varphi, 0)$. The relationships are

$$\mathbf{r} = \rho\mathbf{e}_\rho + z\mathbf{e}_z, \mathbf{r} = R\mathbf{e}'_\rho$$

$$\mathbf{r}' = \rho\mathbf{e}_\rho - R\mathbf{e}'_\rho + z\mathbf{e}_z, d\mathbf{l} = Rd\rho'\mathbf{e}'_\varphi$$

$$\mathbf{e}'_\rho = cos\rho'\mathbf{e}_\rho + sin\varphi\mathbf{e}_\varphi$$

$$\mathbf{r}' = \sqrt{\rho^2 + z^2 + R^2 - 2\rho Rcos\rho'}$$

According to the *Biot-Savart Law*:

$$d\mathbf{B} = \frac{\mu_0 I d\mathbf{l} \times \mathbf{r}'}{4\pi \mathbf{r}'^3} \tag{3.11}$$

where $Id\mathbf{l}$ is the elementary current and μ_0 is the vacuum permeability. In Equation 3.11,

$$d\mathbf{l} \times \mathbf{r} = Rd\rho' \mathbf{e}'_\varphi \times (\rho \mathbf{e}_\rho - R\mathbf{e}'_\rho + z\mathbf{e}_z) = (-\rho R cos\rho' + R^2) d\rho' \mathbf{e}_z + Rz d\rho' \mathbf{e}_\rho$$

Therefore, we obtain the differential form of the magnetic flux density in cylindrical coordinates:

$$d\mathbf{B} = \frac{\mu_0 I'}{4\pi(\rho^2 + z^2 + R^2 - 2\rho R cos\rho')^{3/2}} (-\rho R cos\rho' + R^2) d\rho' \mathbf{e}_z + Rz d\rho' \mathbf{e}_\rho) \tag{3.12}$$

$\mathbf{B}$ has three components in three directions. We only give the component in the z direction:

$$\mathbf{B}_z = \frac{\mu_0 I}{4\pi(r^2 + R^2)^{3/2}} \int_0^{2\pi} \frac{-\rho R cos\rho' + R^2}{(1 - \frac{2\rho R}{r^2 + R^2} cos\rho')^{3/2}} d\rho' \tag{3.13}$$

We only require a magnetic field along the central axis of the ring current for the estimation, therein requiring $\rho = 0$ and $r^2 = z^2$. Therefore, the denominator of the integral on the right-hand side of the formula is equal to 1, and the numerator is equal to R^2. The magnetic flux density of the z component is

$$\mathbf{B}_z = \frac{\mu_0 I R^2}{2(r^2 + R^2)^{3/2}} \tag{3.14}$$

Our electromagnetic field estimation is based on Equation 3.13. Assume that N is the number of coils, which is also the number of rings. Let P point along the surface of

the center, where $r = 0$. Our equation becomes

$$\mathbf{B}_z = \frac{N\mu_0 I}{2R} \tag{3.15}$$

The required magnetic flux density is $\mathbf{B}_z = 0.12$ T. Considering the possibility of actual industrial production, our radius of the ring is $R = 0.05$ m, the number of coils is $N = 400$, and $\mu_0 = 4\pi \times 10^{-7}$ H/m. We substitute these parameters into Equation 3.14 to obtain the current I, which is approximately 29 A. This ideal current is the minimum required input to the electromagnet unit to achieve the desired magnetic flux density. Considering actual production, the coils cannot be arranged closely, and eddy current interference is generated; our input current must be greater than this value.

3.4.2 Pulse Power Supply

The excitation of the electromagnetic unit is provided by the uni-polar pulsed power source. The excitation provides the rectangular shape of the current to the electromagnetic unit. The excitation is also very important, as it directly effects the output of the electromagnet. As discussed in Section 3.4.1, the output current of the pulsed power supply should be larger than 29 A to achieve the desired magnetic field intensity. The current is very large compared to the current used in daily life (0-10 A). Therefore, we cannot directly use ordinary power sources to generate pulses, nor can we use ordinary pulse signal generators used in the laboratory.

The overall design of the excitation source is described in Figure 3.12. We use the design idea of a commonly used capacitive pulsed power supply [22]. A large power storage capacitor is utilized as secondary energy storage. A sufficiently large output current is generated by charging and discharging the capacitor. Based on the capacitor, the PWM controller is used to control the discharge frequency of the power module of the circuit and generate the waveform at the corresponding frequency [20]. The cooling

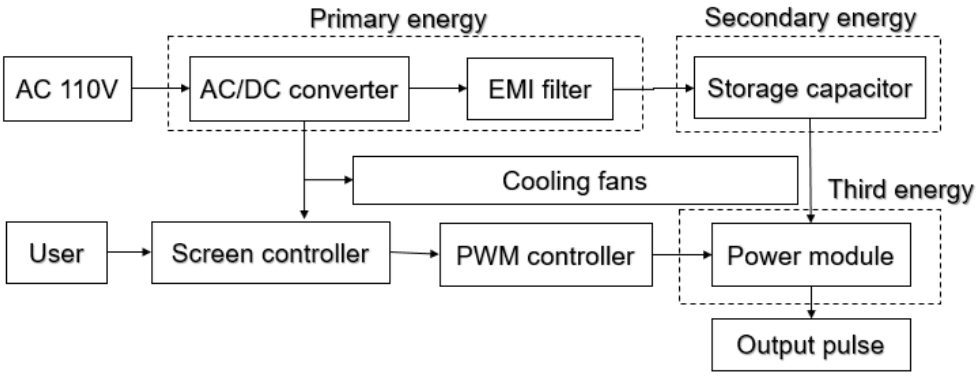

Figure 3.12: Block diagram of the pulsed power supply.

fans are used to cool the high-power power supply.

The input AC electric power of the pulsed power source is 110 V, with a frequency of 60 Hz. The three-phase AC current passes through the AC/DC converter and becomes DC. Then, the EMI filter, which is a low-pass filter, blocks high-frequency electromagnetic interference [12]. The secondary energy is obtained by saving energy from the primary energy source using a large capacitor. The third energy source utilizes the secondary energy source to form an output pulse wave. The designed circuit diagram is shown in Figure 3.13. In the circuit, PSC is the large capacitor. In addition, the other capacitor prevents interference and reduces signal jitter. R1 to R3 are the branch protection resistances. The diodes play a role in preventing the reversal of the current, which can avoid the current causing BJT overheating.

The NPN bipolar junction transistors (BJTs) form the power module. An NPN BJT is shown in Figure 3.14. This is a Darlington transistor [10]. This transistor is equivalent to a contactless switch controlled by the base current i_{b1}. When $i_{b1} = 0$, it is equivalent to an "off" switch, and when $i_{b1} > I_{saturation}$, the switch is "closed". Therefore, we can use the PWM signal from the control module to adjust the frequency of the output waveform [20]. The Darlington transistor is also called a composite triode. The transistor uses a composite connection to connect the collectors of two or more triodes, and the emitter of the first triode is directly coupled to the base of the second

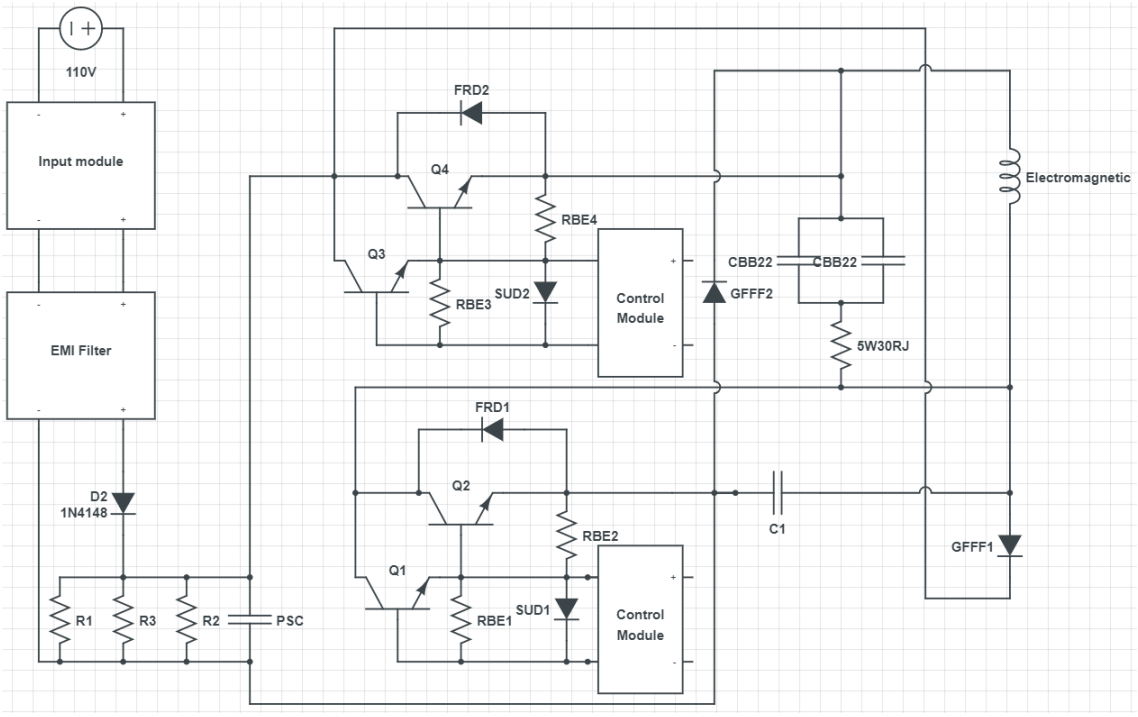

Figure 3.13: Circuit of pulsed power supply .

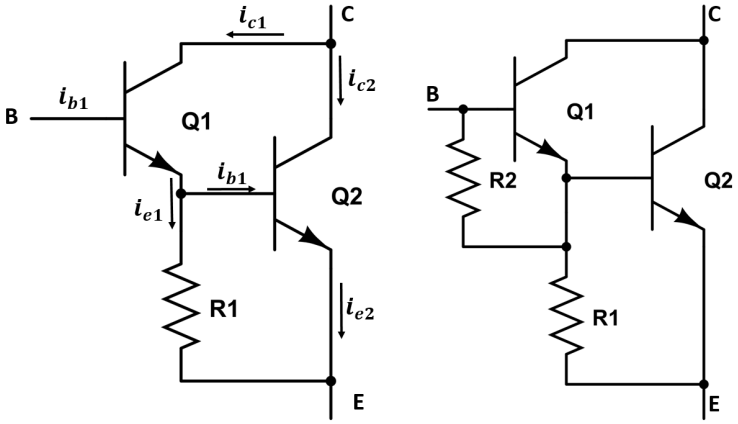

Figure 3.14: Darlington transistor (left) and Darlington transistor with balanced resistor.

triode [24]. This is connected and ultimately fed to three electrodes: E, B, and C. The Darlington transistor has a high current amplification factor. The factor is the multiplication of the factor of each transistor. In Figure 3.13, the left structure can only be used under low power. As the power increases, the pressure drop of the transistor itself causes the temperature to rise. The leakage current of the front-stage transistor (I_{CEO}) will also be amplified step by step, resulting in the overall thermal stability of the Darlington transistor being poor. To mitigate this situation, balanced resistors (R2) are placed inside the high-power Darlington transistor. This will not only greatly improve the thermal stability of the tube but also effectively improve the withstand voltage of the last-stage power transistor. Most high-power Darlington transistors have a damper diode (FRD1) connected in parallel between the collector and emitter of the last transistor to prevent the transistor from breaking down when the load suddenly loses power.

To control the transmission of the base current to control the power module, our control module generates an appropriate PWM square wave to control the frequency of the waveform according to the demand. There are two main types of PWM controllers: a voltage control type and a current control type. Although the voltage-type controller circuit is simple, it is not as accurate or stable as the current controller.

The current control mode in Figure 3.15 is a control method for timing turn-on and peak current turn-off. The error signal V_R is sent to the PWM comparator. The latch is set by an oscillator with a certain frequency, and the latch is reset by the output of the PWM comparator. When the latch state is high, the switch turns on.

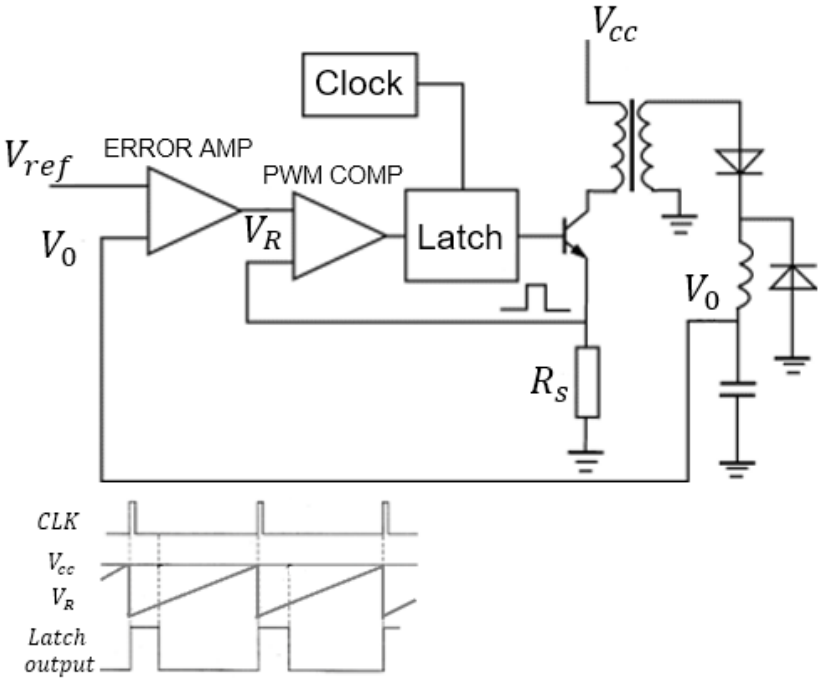

Figure 3.15: PWM control circuit.

Chapter 4

Simulation

The finite element method is a numerical method that has been widely used in numerous applications. It provides solutions to mathematical physics problems based on variational principles. Problems based on continuous objects are transformed into finite nodes for calculation. This method solves problems consisting of continuous geometries and complex material properties and is a powerful computational tool for solving numerous other problems.

The structural parameters of electromagnets have different degrees of influence on their characteristics. The traditional method only determines the parameters of the elec-

tromagnet structure through empirical formulas. In particular, the design of structural parameters that have a major impact on the characteristics of the electromagnet is often not scientific and accurate. Therefore, combined with finite element analysis software for electromagnetic fields, the key parameters and parameters that cannot be determined by empirical formulas are used to simulate and analyze the influence of the electromagnet characteristics. This is necessary to improve the structure, determine the parameters and achieve resource and cost savings.

4.1 Simulation Methodology

ANSYS Maxwell [6] is powerful FEM simulation software that utilizes finite element discretization and Maxwell's differential equations. This software is accurate, easy-to-operate, professional and powerful simulation analysis software. ANSYS Maxwell provides a desktop graphical user interface environment that allows users to build 2D and 3D models easily while viewing the model interactively.

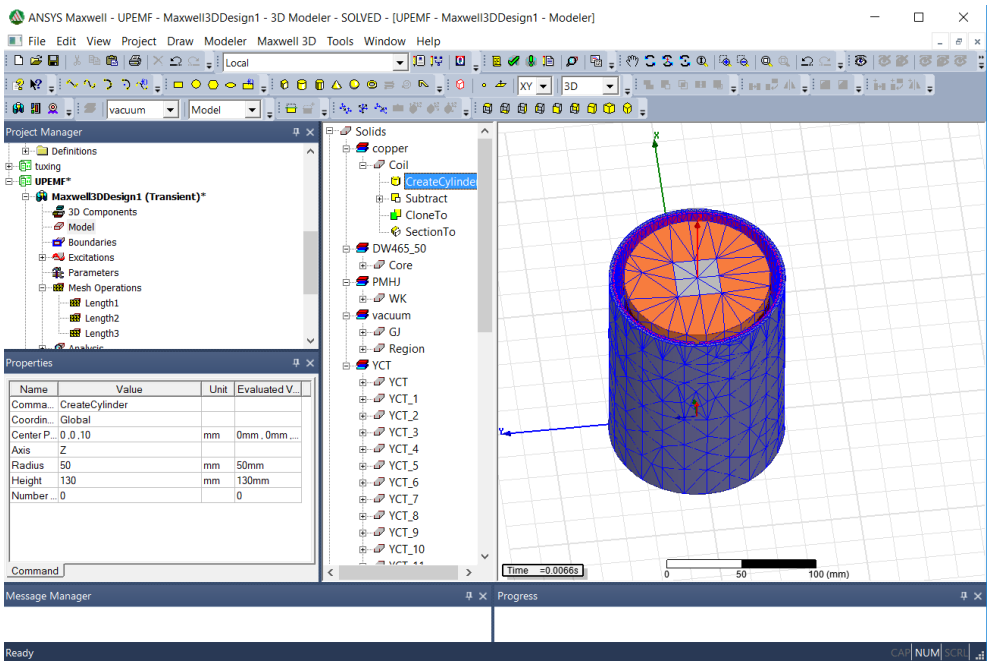

Figure 4.1: ANSYS Maxwell desktop environment

The modeling processes involved in simulating and analyzing a problem are easy to interact with via the user interface, which includes the following steps:

- *Solver setting:* select a proper solver type.
- *Model building:* create the desired geometry model in either 2D or 3D.
- *Material setting:* assign the materials to the geometry model. Users can define their own material or
- *Boundary conditions setting:* set the conditions for the solution of the differential equations.
- *Excitation setting:* set the excitation source parameters of the electromagnetic model such as the current and voltage.
- *Mesh setting:* set the number of nodes and size of the mesh for the calculation.
- *Result setting:* the simulation results are post-processed using, e.g., figure plotting.

4.2 UPEMF Simulation Modeling

The finite element method is an extremely widely used numerical method. Based on the Maxwell simulation software, we first give the differential form of the electromagnetic field to describe the model mathematically in Section 4.2.1. The *Maxwell equations* in differential form are introduced. Then, we give the constitutive relationship and necessary relational expressions. Finally, we give the boundary conditions for calculating the elements. In the remainder of this chapter, the geometric model of our UPEMF apparatus is built and visualized. The simulation process and the results are also presented.

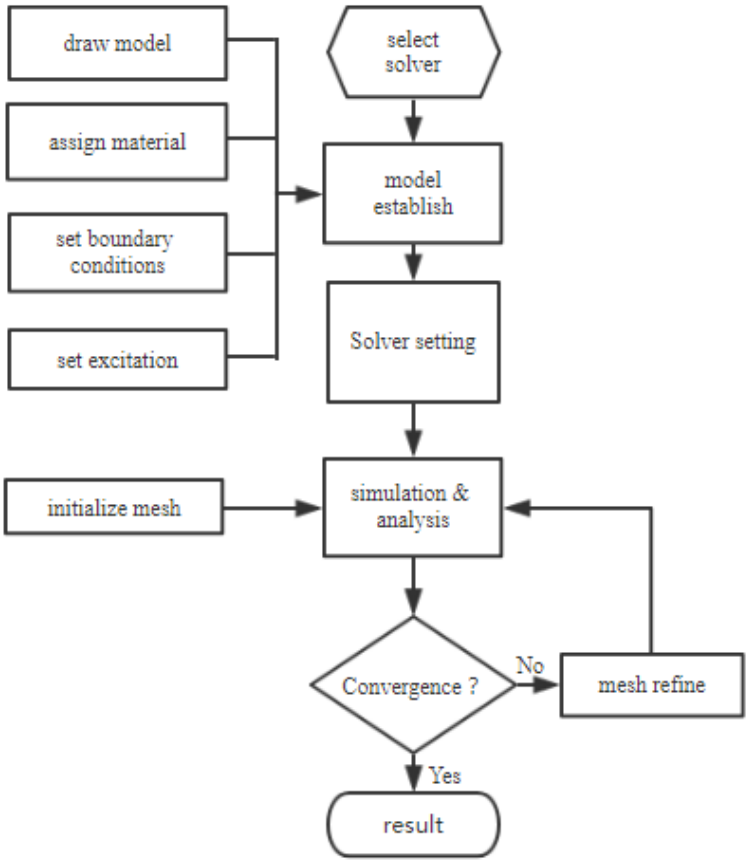

Figure 4.2: A diagram of the ANSYS Maxwell emulation process

4.2.1 FEM Model of Electromagnetic Field

Maxwell's equations quantitatively describe the electromagnetic interactions and the corresponding laws of motion. The equations are the basic theory for studying all macroscopic electromagnetic problems [14]. Simultaneously, they are the theoretical basis and starting point for the finite element analysis of electromagnetic fields.

In the common magnetostatics condition, the current is considered static. According to Stokes' theorem, we obtain Ampere's law and Faraday's law in point (differential) form:

$$\nabla \times \mathbf{J} = 0 \tag{4.1}$$

$$\nabla \times \mathbf{E} = 0 \tag{4.2}$$

In contrast to static magnetic field, the study of which is also called magnetostatics, Maxwell's equations modified *Ampere's law* and *Faraday's law* [7]. Combined with *Guass's law*, Maxwell's equations in differential form are written as follows:

$$\nabla \times \mathbf{H} = \mathbf{J} + \frac{\partial \mathbf{D}}{\partial t} \tag{4.3}$$

$$\nabla \times \mathbf{E} = -\frac{\partial \mathbf{B}}{\partial t} \tag{4.4}$$

$$\nabla \times \mathbf{D} = \rho \tag{4.5}$$

$$\nabla \times \mathbf{B} = 0 \tag{4.6}$$

In these equations, the symbols denote the following:

H is the magnetic field vector (A/m);

J is the current density vector (A/m^2);

D is the electric flux density (C/m^2);

E is the electric field (V/m);

B is the magnetic flux density (T);

∇ is the nabla operator, which defines the curl operation; and

ρ is the volumetric charge density (C/m^2);

Maxwell's equations reveal the relationship between each physical quantity. We assume that a vector and its derivatives are continuous. Then, constitutive equations are introduced to help solve the equations. The constitutive equations describe the relation between physical quantities to make a general solution possible [5].

In a linear, homogeneous, and isotropic medium, the constitutive equations are

$$\mathbf{D} = \varepsilon \mathbf{E} \tag{4.7}$$

$$\mathbf{B} = \mu \mathbf{H} \tag{4.8}$$

$$\mathbf{J} = \sigma \mathbf{E} \tag{4.9}$$

where ε is the permittivity (F/m), μ is the magnetic permeability (H/m), and σ is the electric conductivity ($1/\Omega m$).

The magnetic permeability measures the ability of a material to establish magnetic fields within itself. The vacuum permeability is defined as $\mu_0 = 4\pi 10^{-7} (H/m)$. The permeability of the other materials is defined as the relative permeability of vacuum such that

$$\mu = \mu_0 \mu_r \tag{4.10}$$

Materials with higher permeability allow magnetic field lines to pass through more easily

than materials with lower permeabilities. In practice, iron, nickel and alloys have high permeabilities. It is also considered as a selection criterion when choosing the magnetic core and shield.

The magnetic flux density $\mathbf{B}$ in terms of the magnetic vector potential $\mathbf{A}$ is defined as

$$\mathbf{B} = \nabla \times \mathbf{A} \tag{4.11}$$

The general expression for $\mathbf{A}$ in terms of the volumetric current density $\mathbf{J}$ is

$$\mathbf{A} = \frac{\mu_0}{4\pi} \int_v \frac{\mathbf{J}_v dv}{R} \tag{4.12}$$

where $\mathbf{J}_v$ is the volumetric current density and R is the resistance.

For solenoids excited by a current, the current density is described as

$$\mathbf{J} = \frac{N I_{coil}}{\mathbf{A}} \mathbf{e}_{coil} \tag{4.13}$$

where e_{coil} is the unit vector of the coil. The amplitude of the current in the coil is the rectangular waveform described in Chapter 3 as

$$I_{coil} = X_r(t) = \begin{cases} \text{A},\ 0 < t < t_1 \\ 0,\ t_1 < t < T \end{cases}$$

In addition to the above Maxwell's equations and constitutive equations, defining boundary conditions are the last step in solving electromagnetic field problems. [7] The differential form of Maxwell's equations requires that there should always be an open neighborhood around the point of action. Otherwise, the vector fields $\mathbf{E}$, $\mathbf{D}$, $\mathbf{B}$ and $\mathbf{H}$ will not be differentiable. In other words, the medium must be continuous. This means that Maxwell's equations cannot be used at the interface of two different media with different permittivities and permeabilities. As a result, the boundary conditions must be

defined before calculating the physical quantities on the boundary.

For electric fields, the boundary condition is

$$\mathbf{a}_{12} \times (\mathbf{E}_1 - \mathbf{E}_2) = 0 \tag{4.14}$$

where $\mathbf{a}_{12}$ is the unit vector at the interface pointing from medium 1 to medium 2. This condition states that the tangential component of $\mathbf{E}_1$ and $\mathbf{E}_2$ is continuous on both sides of the interface.

For electric displacement fields, the boundary condition is

$$\mathbf{a}_{12} \times (\mathbf{D}_1 - \mathbf{D}_2) = \rho_s \tag{4.15}$$

where ρ_s is the surface charge. This condition states that the normal component of $\mathbf{D}_1$ and $\mathbf{D}_2$ has a surface charge at the interface surface. If there is no surface charge at the interface, the normal component is continuous.

For magnetic fields, the boundary condition is

$$\mathbf{a}_{12} \times (\mathbf{B}_1 - \mathbf{B}_2) = 0 \tag{4.16}$$

This condition states that the normal component of $\mathbf{B}_1$ and $\mathbf{B}_2$ is continuous on both sides of the interface.

For the magnetic field strength, the boundary condition is

$$\mathbf{a}_{12} \times (\mathbf{H}_1 - \mathbf{H}_2) = \mathbf{J}_s \tag{4.17}$$

where $\mathbf{J}_s$ is the surface current density. This condition states that the tangential component of $\mathbf{H}_1$ and $\mathbf{H}_2$ at any point on the interface is discontinuous by an amount equal to the surface current density at that point.

4.2.2 Initial Settings and Model Building

Since our design attempts to build a real UPEMF apparatus, 2D simulations are not sufficient. We choose "insert maxwell3D design" to initialize the model building. Since our UPEMF is an AC magnetic field, we need to analyze the field changing with time. Thus, we set "transient" as the solver type. We imported the "RMxprt" as our material library. The "RMxprt" library provides practical parameters for thousands of materials. It is more convenient to use the materials from the library than to search for and set them by ourselves.

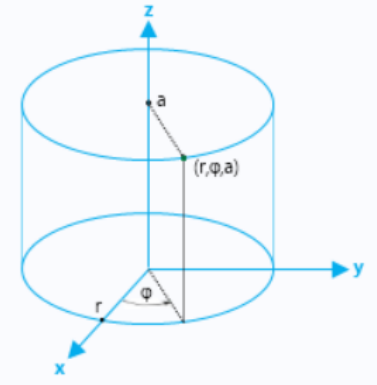

Figure 4.3: Cartesian and cylindrical coordinates.

The geometry model is built in the Maxwell desktop environment. The unit of measure is set to mm. Two sets of coordinates are defined for the model (Figure 4.3): Cartesian and cylindrical coordinates. The Cartesian coordinates are used as the global coordinates. It is convenient to draw the model in Cartesian coordinates. The cylindrical system is adopted when setting the magnetization direction along the radial direction.

We set the origin as the south end of the magnetic core. The magnetic core is built using cuboids. Cylinders are used to build the coil skeleton, coils, and magnetic shield in Figure 4.4. The coil skeleton support the coils. The magnetic shield covers the electromagnet as the outer layer. The ring structure is built by subtracting two cylinders with different radii.

In practice, a permanent magnetic ring with radial magnetization and with our size,

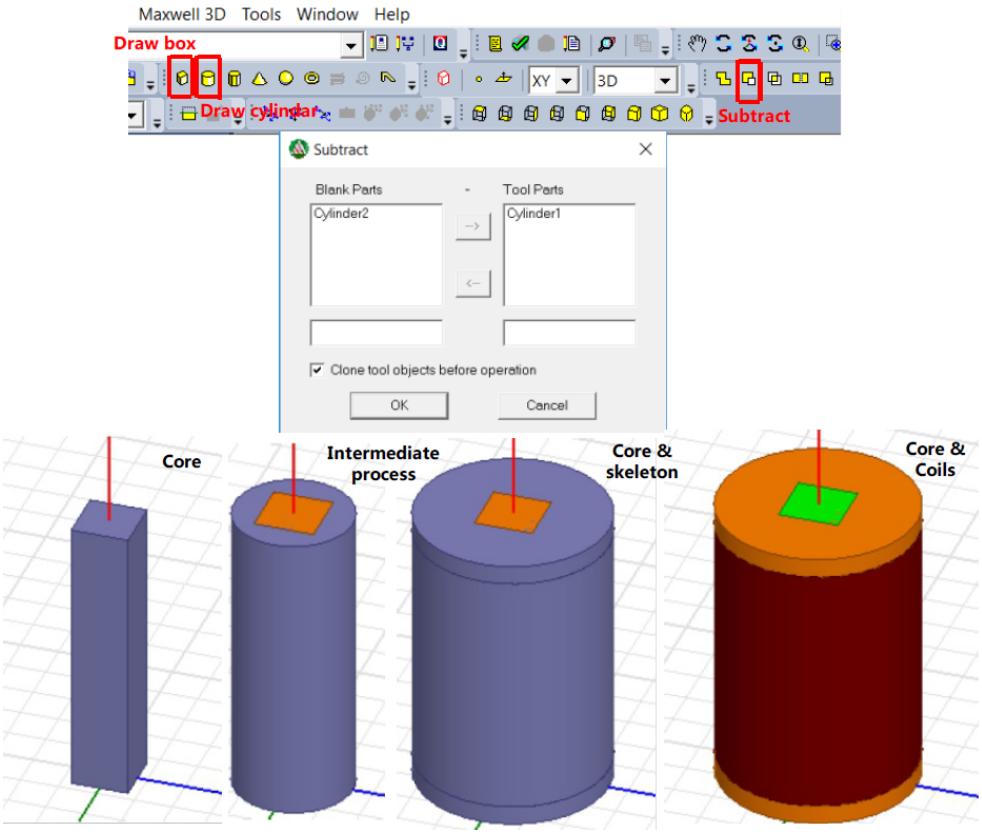

Figure 4.4: Geometry building plane and process.

as we need to cover all sides of the electromagnet, is very difficult to produce; thus, it is too expensive to customize. Thus, we sacrificed the performance of the concentrator and found an alternative. In our simulation in Figure 4.5, the concentrator consists of 34 permanent magnets, which are closely positioned next to each other. Each permanent magnet is a prolate cuboid. The length, width, and thickness are 50 mm, 10 mm, and 1.5 mm, respectively. The ring is duplicated by a single cuboid. The mirrors are produced along the z-axis. Each mirror occupies an angle of $360 \times \frac{1}{34} = 10.58$ degrees.

The 2D sectional view from the y-z plane is shown in Figure 4.6. The final 3D structure of the electromagnet is shown in Figure 4.7.

4.2.3 Implementation of AC Magnetic Field in Maxwell Software

The geometry model was generated before we assigned the proper materials. The materials are adopted according to the real materials that we used in the implementation step. The materials and the main simulation parameters are shown in Table 4.1. As we mentioned in Section 4.2.1, we assume that the media are linear, homogeneous, and isotropic. However, many materials that we use in the real world are nonlinear. Therefore, the constitutive equations of these nonlinear materials are nonlinear.

To generate a more accurate model, we imported the H-B curve as the constitutive equations, which describes the relation between the magnetic flux density and the magnetic field intensity. The H-B curves replace the constitutive equations in Equation 4.8. The setting of the H-B curve of the magnetic core and shield are displayed in Figure 4.8 and Figure 4.9.

Our concentrator consists of permanent magnets. Each magnet is magnetized. This magnetic property can be described with a magnetization vector.

$$\mathbf{M} = \frac{\mathbf{B}}{\mu_0} - \mathbf{H} \tag{4.18}$$

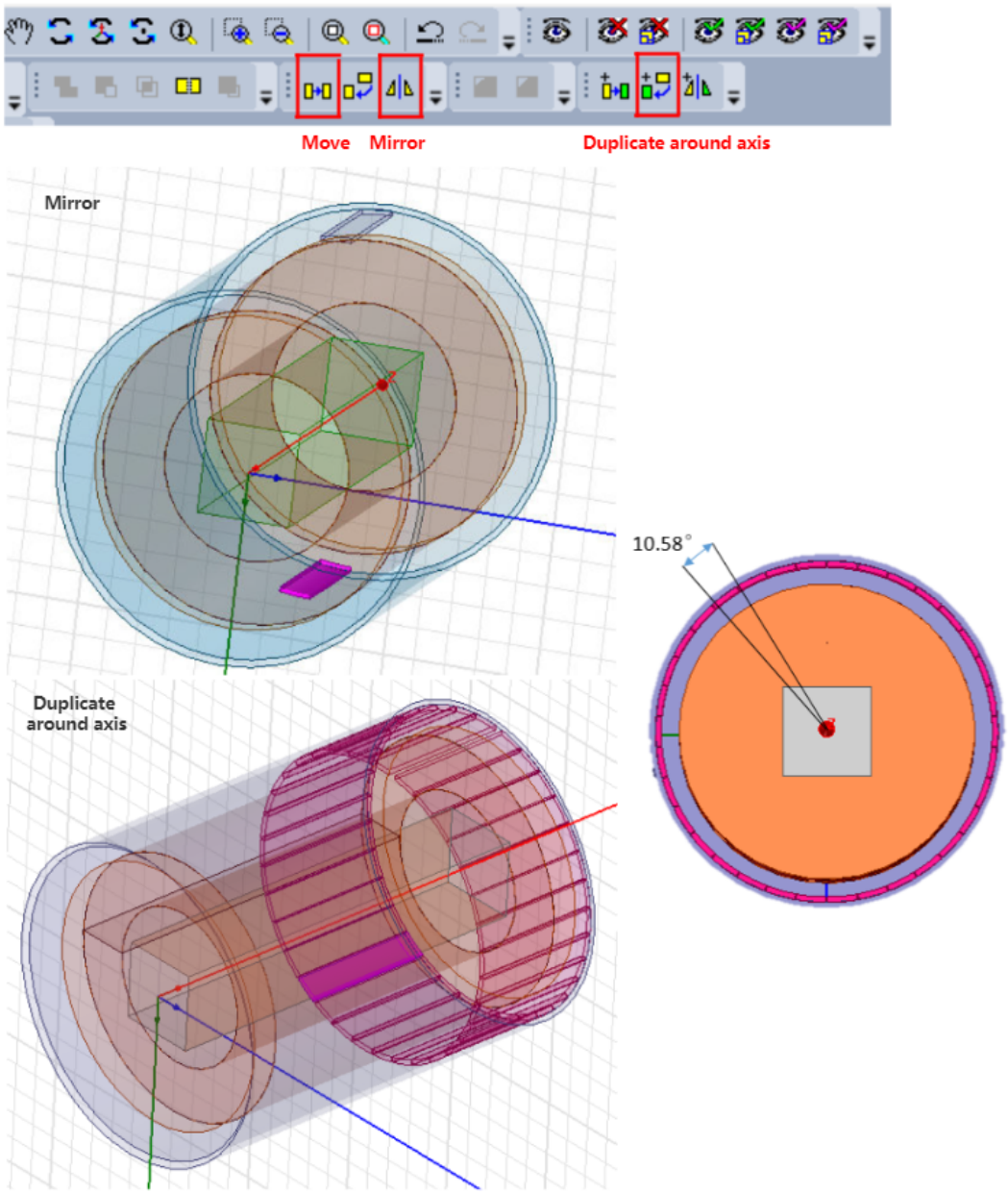

Figure 4.5: Process of creating the geometry of the concentrator.

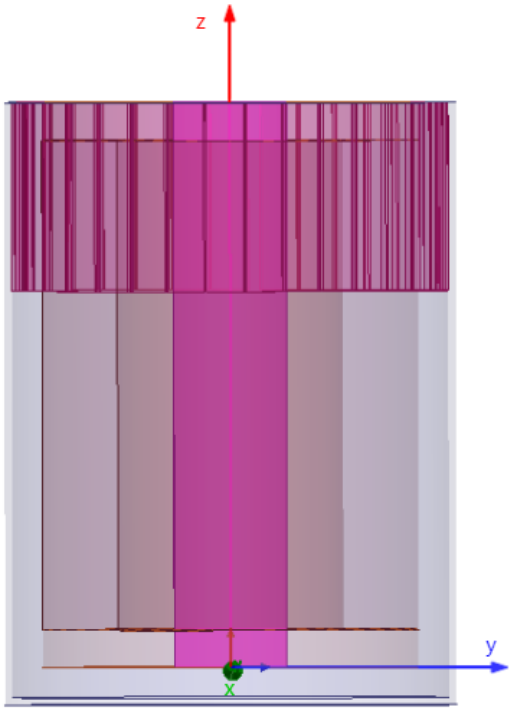

Figure 4.6: UPEMF electromagnetic geometry model 2D sectional view.

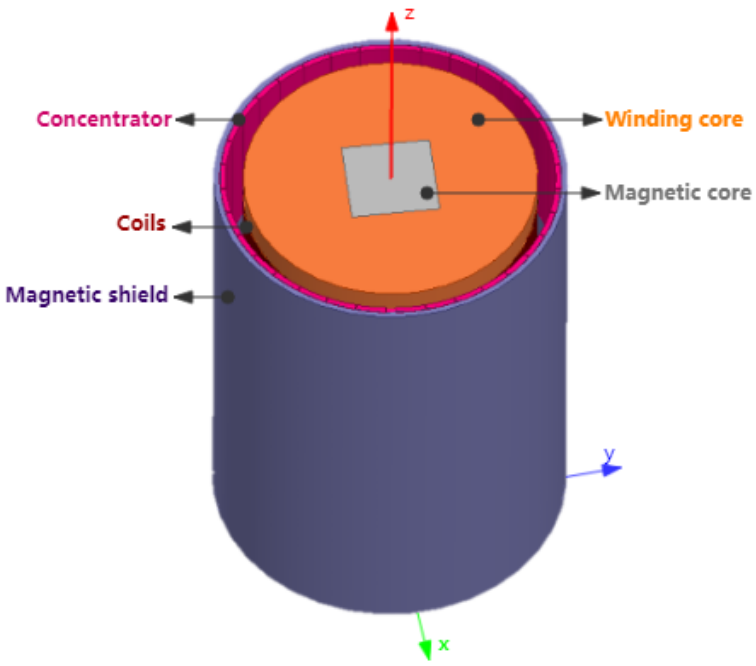

Figure 4.7: UPEMF electromagnetic geometry 3D model structure.

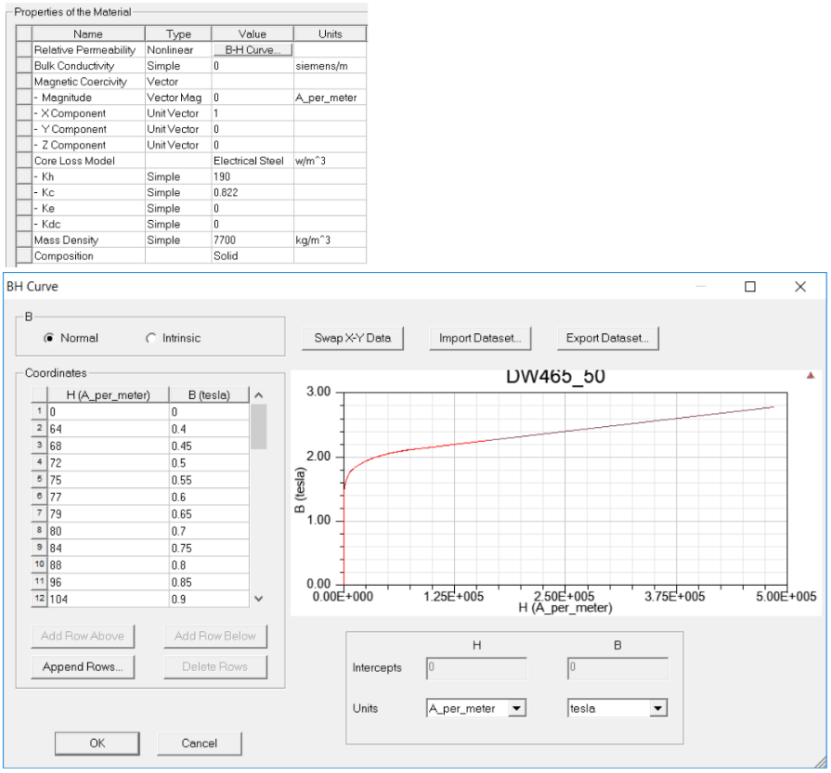

Figure 4.8: H-B curve of magnetic core and parameters of silicon steel sheet.

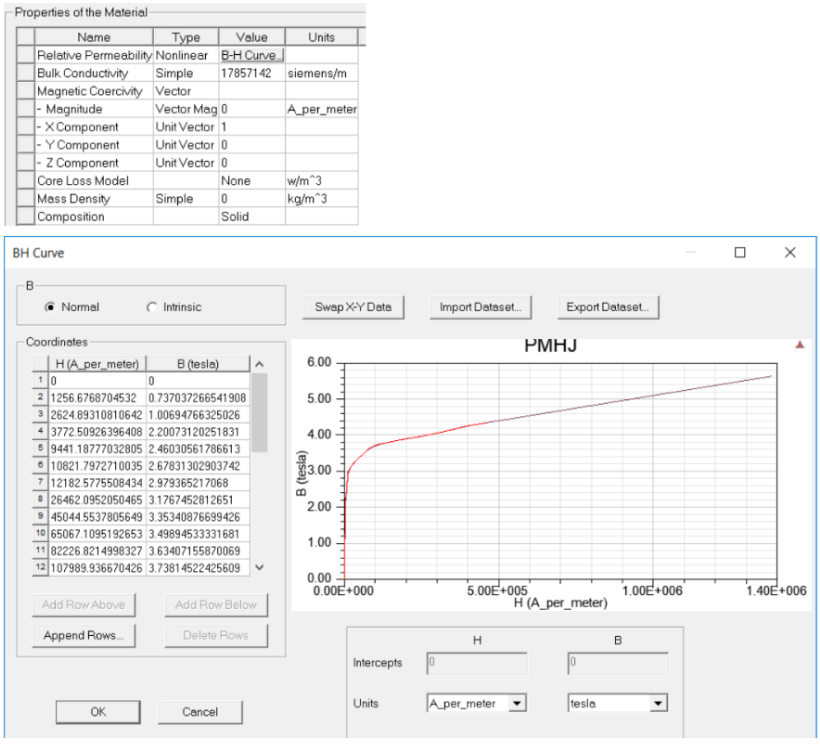

Figure 4.9: H-B curve of magnetic shield and parameters of Mu-metal.

Table 4.1: Summary of the simulation parameters.

Components	Material	Dimension	Key Physics Properties
Core	Silicon steel	Height: 150 mm Side length: 30 mm	HB curve*
Coil	Copper	Height: 140 mm Diameter: 2 mm Turns: 414	Current capacity: [-50A, 50A]
Concentrator	NdFeB	Height: 150 mm Thickness: 1.5 mm	Remanent magnetization: 0.1415T Direction: -r
Shield	Mu-metal	Height: 160 mm Thickness: 1 mm	HB curve* Relative permeability: 80,000

The calculation of the field should follow this constitutive equation. The initial background potential **A** is set to 0, as we simulate the electromagnet in an environment without other electromagnetic fields. The excitation of the winding coils is added at the surface. The winding coil number is set to 414. We added a solution setup and set the time step and duration of the simulation.

4.2.4 Mesh Setting

Mesh division is a method of FEM modeling for breaking up a large simulation problem into small elements. Each small element is a geometric body composed of nodes. A typical shape of an element is a tetrahedron. Nodes are the endpoints, vertices, or specific points of the element geometry. The physical changes of the cells are reflected in the nodes. The FEM calculates the physical quantities of each individual element and then assembles the discrete domain of the elements into the total matrix equation (combining equations). The assembly is performed at the adjacent nodes. After assembling, the approximate solution is calculated. The initialization of the mesh is very important. Higher mesh resolutions result in more accurate results. However, the computational complexity increases with accurate meshes. If the mesh resolution is larger, the software takes more time to converge. If the mesh does not meet the calculation requirements

of the combined equations, the mesh should be of higher resolution, thus constituting a trade-off problem. Since there are many edges and small phases in our electromagnetic model, the magnetic fields are calculated in many small elements. Therefore, we use a dedicated mesh and set the default mesh as the initial mesh.

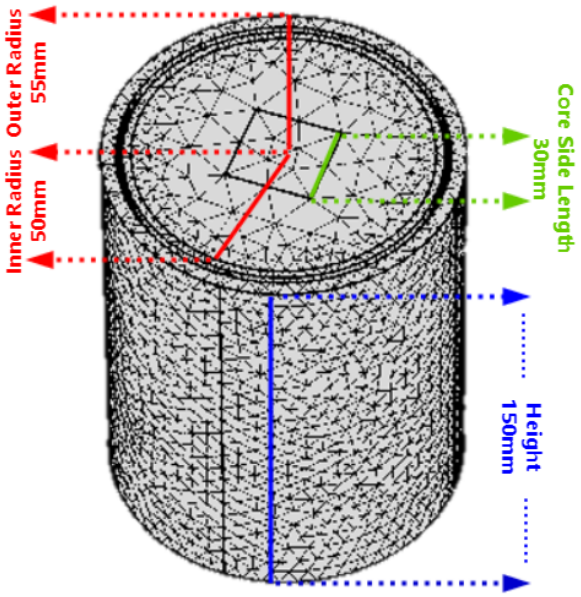

Figure 4.10: Mesh setting visualization.

When we use the rule of splitting the interior of an object to divide it, we need to set the maximum length of the cell or the maximum number of cells. The maximum number of units is the maximum number of triangulated elements in the selected mesh. By setting these parameters, we can limit the maximum number of model partitioning units in the software during refinement, thereby avoiding excessive memory usage for untidy units. To achieve good calculation results and reduce the calculation time, we choose to manually set the maximum side length of the grid. After numerous experiments, we chose the maximum length of the triangulation unit of the shell and the skeleton to be 0.5 mm, the maximum length of the triangular unit of the core is 2 mm, the maximum length of the triangular unit of the coil is 4 mm, and the triangulation unit of the solution area is the largest. The side length is 5 mm. The final mesh is shown in Figure 4.10.

4.3 Simulation Results and Analysis

Post-processing is the last step in the simulation process after calculation. In this process, we created the transient reports of the input current, eddy losses of the shield and the magnetic flux density at a point on the north pole in Figure. To visualize the results, cloud maps of the magnetic flux density (Figure 4.13) and eddy losses (Figure 4.14) are drawn. These two graphs display the physical quantities of the model.

From Figure 4.11, we can clearly see the relation between the input current and the produced magnetic field. The input current exciting the coils has a peak value of 45 A, which is huge compared to common household appliances. The duration for one cycle is set to 0.0334 ms based on the 30 Hz requirement. Considering the problem of power consumption, the duty cycle should be close to 0. A duty cycle close to one means that the power excitation provides more energy to maintain the peak value of the current to a greater extent than a lower duty cycle. Our motivation and requirements reveal that a longer duration for a peak value does not provide greater benefits. Therefore, a larger duty cycle is superfluous. To avoid wasting power and reduce the difficulties in achieving a huge power excitation, the zero value duration is set to 0.028 ms, and the peak duration is set to 0.0054 ms.

The magnetic flux density is measured at the top of the magnet at the center of the y-z plane as a point model, as shown in Figure 4.12. We created a point element on the surface for convenience. Note that the material and physics for the magnetic disc are not specific. We only use them to represent the result when performing post-processing. The performance of the end-point magnetic field is important, as it is the emitting end at the north pole. Patients will directly benefit from the UPEMF wave produced at the north pole's surface. From the graph of the end-point magnetic field, we can see that the curve is not regular, as is the curve in the input current. In the first period, the strength initially increases up to 0.20 T. Then, the strength decreases quickly at the 0

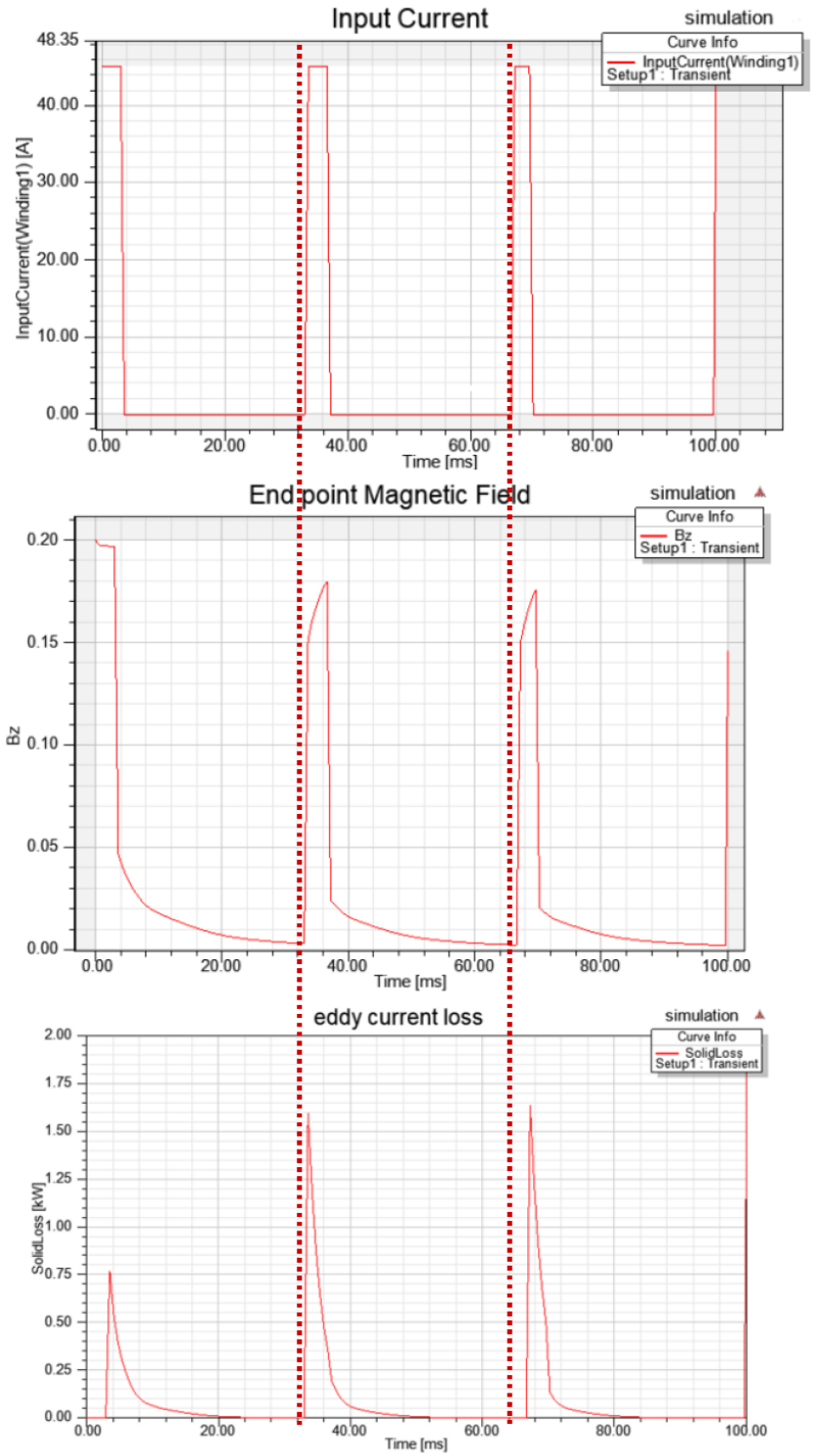

Figure 4.11: Maxwell simulation of the designed electromagnetic unit. The unit is stimulated using an input current (top). The end point magnetic field flux density (middle) shows the north pole output. The eddy current losses (bottom) represent the energy waste caused by inductance.

value duration of the input current. However, there is an obvious falling process. The falling process is causing by the inductance. Inductance is a property of an electrical conductor that opposes a change in current. As a result, our UPEMF wave will not be an ideal rectangular wave. In the second period, the strength rapidly reaches 0.15 T and then slowly rises to a maximum value of 0.18 T, but not 0.20 T, during the peak input current duration. The delay effect of this rising and falling of the magnetic field and the loss of the maximum value reveal the resistance and power consumption. In the simulation step, we set the parameters and satisfy the requirements above 0.12 T, instead of at 0.12 T, to ensure that the real implementation can achieve 0.12 T.

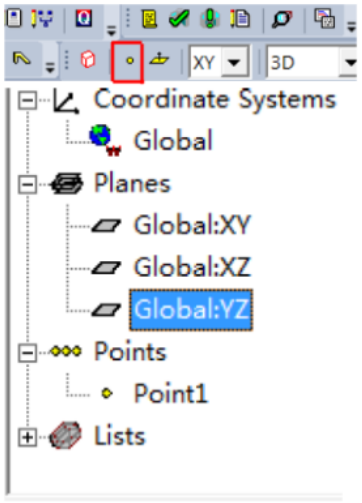

Figure 4.12: Point model for measuring magnetic flux density at the north pole.

In the cloud map of the magnetic flux density (Figure 4.13), the rainbow colors reflect the different densities of **B**. From dark blue to dark red, the density increases. The map shows that the highest density appears in the internal magnetic core and the shield. The materials of these two structure all have high relative permeabilities. They provide paths for the magnetic induction lines with lower resistance. Thus, the magnetic induction density is high. Outside the magnetic shield, the magnetic flux density is close to 0 T. The field on the south pole (bottom) is eliminated.

Eddy currents are loops of electrical current induced within conductors by a changing

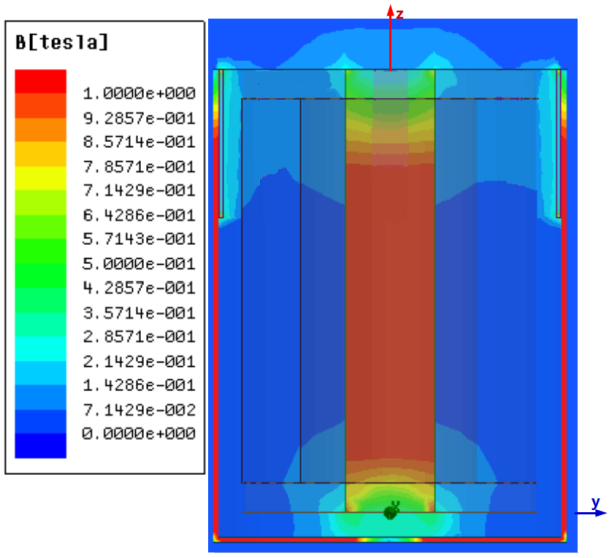

Figure 4.13: Cloud map of magnetic flux density.

magnetic field ($\frac{\partial \mathbf{B}}{\partial t} \neq 0$) in the conductor due to *Faraday's law* of induction [46]. Our UPEMF is an AC electromagnetic field. Therefore, the strength of the field changes with time. Thus, the generation of eddy currents is inevitable. The magnitude of the eddy currents is given by

$$I = \frac{-1}{R}\frac{d\Phi_B}{dt} \tag{4.19}$$

where R is the resistance of the material and Φ_B is the flux at any instant (t) going through the surface of the material. Φ_B is calculated by *Faraday's law*:

$$\Phi_B = \int_s \mathbf{B} d\mathbf{s} \tag{4.20}$$

The direction of the eddy currents is given by *Lenz's law* or *Fleming's right-hand rule*.

In Figure 4.14, the eddy current loss is shown on the bottom. Corresponding to the graph above, we can clearly see that the maximum value of the eddy current loss appears when the changing rate of the input current is maximized. In the simulation, the instantaneous eddy current loss can be as high as 1.6 kW, which is very high. The cloud map of eddy losses shows that the highest loss occurs on the structure with the highest

magnetic flux density. Increases in temperature occur due to increases in internal energy. In our case, we need to reduce the high eddy currents to reduce heating problems, which should not be ignored. Because our model does not consider the individual structures of each part, such as the slot in the silicon sheet and the impurities of the materials, high losses are reasonable. However, when we actually develop the electromagnet, high-resistance materials and structures will be utilized.

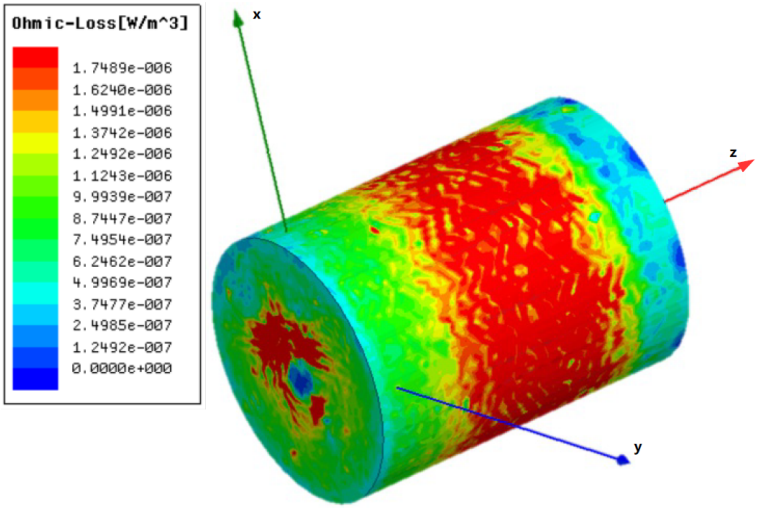

Figure 4.14: Cloud map of eddy losses.

Chapter 5

Implementation and Results

In this chapter, we present the details of the implementation of our UPEMF apparatus. In Section 4.1, we discuss the magnetic unit implementation, which includes the actual shape and materials of each part and the parts combined together. In Section 5.2, the structure of a pulsed power supply is introduced. The components of the pulsed power supply are introduced and analyzed. Section 5.3 presents the evaluation results of our UPEMF apparatus. The output waveform of the pulsed power supply and the electromagnetic unit are displayed and analyzed.

5.1 Electromagnetic Unit

The magnetic unit is developed based on the simulation parameters and the choice of proper materials. The magnetic core is show in Figure 5.1. The magnetic core is

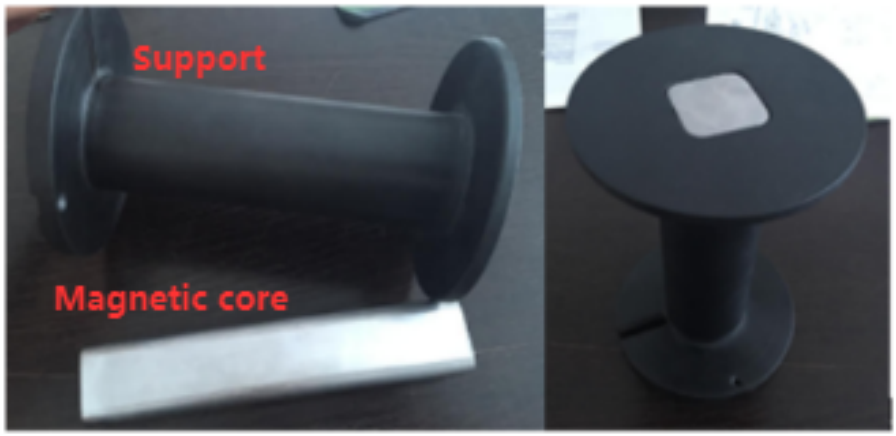

Figure 5.1: The support and magnetic core.

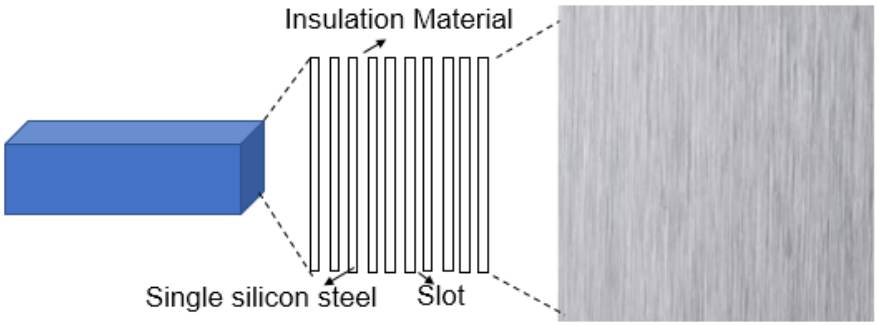

Figure 5.2: Silicon steel sheet.

composed of a silicon steel sheet, as shown in Figure 5.2. A typical silicon steel has a silicon content of approximately 0.5% to 4.5%. Several individual silicon steels are combined using slots of insulation material. The thickness of each silicon steel sheet is approximately 0.1 mm to 0.25 mm. The production method of this material is cold rolling. There are two types of silicon steels. The first type is non-oriented silicon steel, with 0.5% to 3.0% silicon content [30]. The other type is oriented silicon steel, with a

silicon content of over 3.0%. Compared to their process, the requirements of non-oriented silicon steel are relatively low.

Compared with cold-rolled non-oriented silicon steel, oriented silicon steel presents much lower losses than non-oriented silicon steel. The magnetization has a strong directionality; the easy-magnetization rolling direction has a superior high permeability and low loss characteristics. The iron loss of the oriented strip in the rolling direction is only 1/3 of that in the transverse direction, and the permeability ratio is 6:1. The iron loss is approximately 1/2 of that of the hot strip, and the permeability is 2.5 times the latter [48]. In simple terms, the orientation sheet has a lower iron loss due to its better magnetic permeability than that of the non-oriented sheet. We adopted the oriented sheet as our material to build the magnetic core to further improve the performance.

The black support is composed of plastic, which has no effects on our electromagnetic field because of its lack of magnetization ability. There are two symmetrical holes in the bottom to fix the terminals.

Due to the very large input current (up to 50 A) of our instruments, our coil wire also has to be large. According to the simulation, the coils have 414 turns in total. To withstand the high current, we choose a wire with a maximum outer diameter of 0.3 cm, which is very large compared to common wires. The coil wires that we used are enameled wire. Enameled wire is a typical winding wire, consisting of two parts: a conductor and an insulating layer. The bare wire is softened by annealing and then painted and heated repeatedly.

Since our wire is thick, the number of windings per cm is small. If we wind the wire in one layer, as is typical, the length of the coils would exceed 15 cm, and the output strength of the field would be weaker than desired. Therefore, the coils were wound layer by layer. Since our designed number of coils is 414 and since the length from the inner circle to the outer circle is 3 cm, we used 3 cm$\div$0.3 cm=10 layers in total, each layer being approximately 42 windings.

Figure 5.3: Electromagnetic unit without shielding.

The wound electromagnetic unit is shown in Figure 5.3. To tighten the coils, two plastic rings are added, thus dividing the coils into three parts on the surface. On the surface, the transparent plastic seals the outer coils to provide electrical insulation for safety reasons. At the bottom of the electromagnet, two pieces of copper are connected to the positive (red wire) and negative (black wire) electrodes.

The concentrating ring is produced as shown in Figure 4.5 in Chapter 4. The actual magnetic ring consists of 34 strong permanent magnets, which are closely positioned to each other. The main parameters for each magnet are shown in Table 5.1. The north and south poles are on two bottom sides, which produces a magnetization in the thickness direction. A sintered NdFeB magnet is a strong magnet with a magnetic field density of 1.415 T.

This magnet is made from a rare earth element alloy (NdFeB). In the permanent magnet, rare earth magnets can produce the largest magnetic field, compared to Al-

Table 5.1: Parameters of a permanent magnet

Product Size	Length: 50 mm Width: 10 mm Height: 1.5 mm
Material	Sintered NdFeB
Magnetization direction	Thickness direction
Surface Gauss	1415 Gauss
remanence	12200 Gauss
BH_{max}	35 MGOe

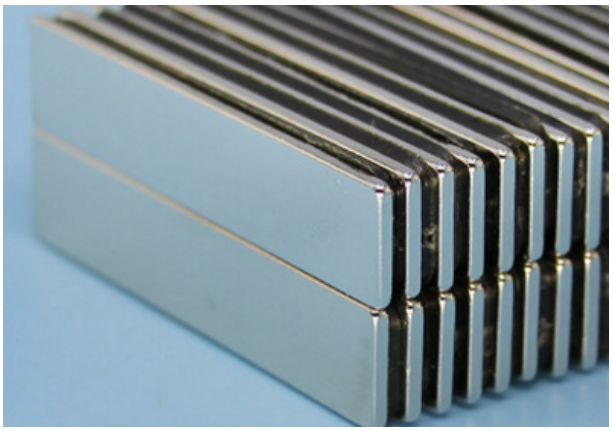

Figure 5.4: Strong magnet sheets for the concentrator.

NiCo magnets and ferrite magnets [13]. Rare earth magnets generally produce magnetic fields in excess of 1.4 T, while ferrite magnets and ceramic magnets only produce fields of approximately 0.5 T to 1 T [28]. Moreover, its crystal structure has a high magnetic anisotropy, which makes it easy to magnetize in a certain direction but difficult to magnetize in other directions. The above characteristics enable the magnet to generate a strong magnetic field while maintaining its original magnetization in our changing magnetic field.

According to the theory from Section 3.3.3 in Chapter 3, we need to choose a material with high permeability for the magnetic shielding.

The high permeability will change with changing shielding magnetic field intensity. When the electromagnetic field strength is low, the magnetic permeability will increase with increasing magnetic field intensity. When the magnetic field strength exceeds a certain limit, the magnetic permeability will be sharply decreased, and magnetic saturation

Table 5.2: Parameters of Permalloy for magnetic shielding

Product Size	Thickness: 1.0 mm length: 320 mm Height: 180 mm
Materials	Ni-Fe alloy; Ni (80.3%) Fe (14.2%) Mo (4.95%)
coercive force	$\leq$2.0 A/m
μ_0	$\geq$60 mH/m
μ_{max}	$\geq$280 mH/m
Resistivity	0.56 $\mu\Omega$m
B_s	0.7 T

occurs at this time in the permeable material, which means that the material has lost its magnetic shielding capability.

The higher the permeability, the easier it is to saturate. Thus, the key to low-frequency magnetic field shielding is to choose a magnetically permeable material with sufficient permeability and saturation characteristics.

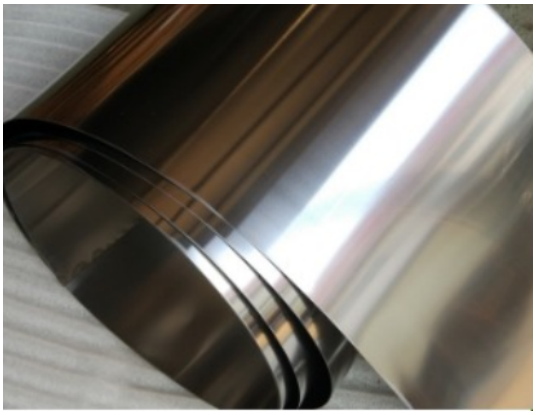

Figure 5.5: Permalloy for magnetic shielding.

Permalloy is our choice for shielding. Permalloy has a very high magnetic permeability. It is a nickel–iron magnetic alloy, with approximately 80% nickel and 20% iron content. To improve the resistivity and improve the performance, Mo is added to the alloy. From Table 5.2, we can see that this material has a saturation magnetic induction (B_s) of 0.7 T, which is acceptable considering the intensity of our electromagnetic wave, and the permeability is high.

The alloy is slowly crimped, closed, and laminated with a non-magnetic plastic adhesive to form a barrel-like ring. In the magnetically shielded inner ring, the permanent

magnets are arranged in the transverse direction, and the longer side of the permanent magnet is placed along the height direction of the magnetic ring. Each permanent magnet needs to be closely placed to ensure the conductive connectivity of the permanent magnet magnetic ring. Each permanent magnet and the magnetic shield ring contact surface are glued together. Finally, the shield of the magnet and the collector of the magnet form a complete structure. Then, the complete structure is installed on the electromagnet, as shown in Figure 5.6. On the bottom of the unit, a flat Permalloy sheet is placed as a base.

Figure 5.6: Magnetic unit with shield and concentrator

5.2 Pulsed Waveform Generator

Our pulsed power supply needs to generate high-power output according to the previous design and requirements. Therefore, the current in the main circuit during the actual production process is very large. Thus, the circuit must be able to sustain large currents and substantial heating during production.

The internal structure of the power supply is shown in Figure 5.7. According to the

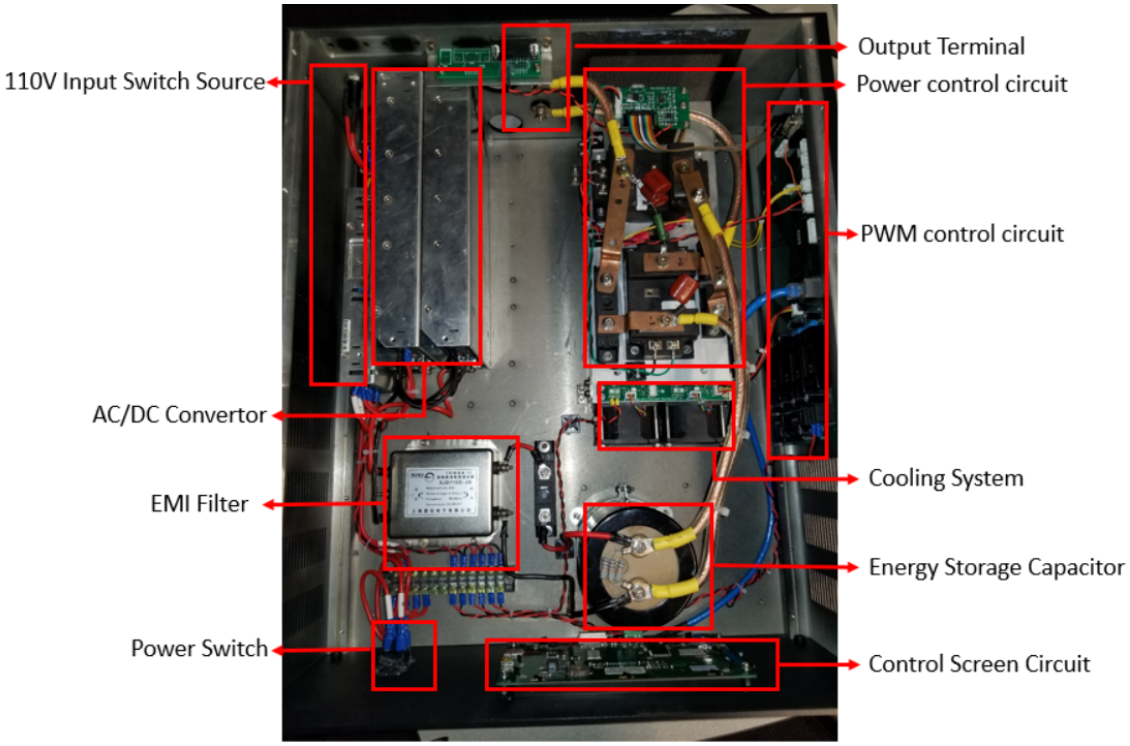

Figure 5.7: Internal structure of the pulsed power supply.

design in Chapter 3, the pulsed power supply is built in the factory. The components are set aside to provide significant space, especially the placement between the three power levels. The interval between the power levels is greater than 5 cm to avoid damage to components due to heat and static electricity.

The main components that we use are shown in detail in Figure 5.8. Among them, we have used diodes that can operate at high currents. These diodes can prevent high reversed currents up to 55 A in breakdown circuits due to the voltage of the electromagnet switching during a sudden power failure. The capacitor that we use is a huge electrolytic capacitor. It can store 22000 MFD; in contrast, regular capacitors are 100 μF to 10 F. The output of the power capacitor can reach 50 A.

The input of the capacitor is connected to an EMI filter. The primary energy is converted to DC through an AC/DC converter and passed through an EMI filter. The connection wire is the main method of interference with the incoming and outgoing

devices. Through the power line, the interference of a previous device can be transmitted to another device and interfere with the normal function of the capacitor. Meanwhile, the interference generated by the capacitor may also be transmitted to the previous device through the wires. The interference signals here are mainly high-frequency AC signals, and our capacitors use DC charging. Thus, the EMI filter here is equivalent to a low-pass filter that filters out high-frequency interference. Therefore, an EMI filter for large currents is installed before the input of the capacitor. In the power control circuit, the power modules [1] are Darlington transistors, as we mentioned in Chapter 3.

The choice of wires for high currents in the circuit is also important. In a high-power circuit, because of the relatively large resistance of thin wires, the heat generated by the current is also greater. According to *Joule's Law*, the heat generated by the current through the conductor is proportional to the current squared, which is proportional to the resistance of the conductor and the energization time: $Q = I^2Rt$. Assume in 1 s that 45 A of current goes through 1 cm of wire with a diameter of 0.2 cm, and the resistance is 65Ω: the heat generated is $Q = 45^2 \times 65 = 2025J$. The heating of components and wires not only affects the performance of the components but also may lead to the destruction of the components. Considering performance and safety, we used two wires with a cross-sectional area of 100 mm^2 to connect the capacitor with the power module. Moreover, the connection inside the power module circuit is made with wide copper plates to sustain large currents.

The two front and rear panels of the pulsed power supply are distributed as touch screen controls and input and output interfaces.

On the front plane (Figure 5.9), the touch screen has four buttons: ON/OFF, pulse width, current and frequency. The desired parameters of the power supply are entered by hand using the touch screen. The indicator light is used to indicate the current state of the power supply. The bright light indicates the amount of power to open. The setting parameters of the pulsed power supply are as follows: 1) the output pulse width setting

Components	Model and Parameters	Appearance
Anti-reverse diode	LJ-MD55A 1600V 	
Power model	FUJI 1DI480A-055 480A, 550V 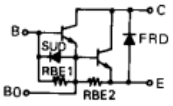	
Power storage capacitor	HCG FA 22000 MFD 250VDC 	
AC/DC convertor	RSP-750-48 10A, 240VAC 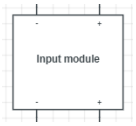	
EMI Filter	SJD710D-20 20A 50/60Hz 250VDC 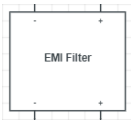	
Control Controller	DC10600RS070- 05CF_RTC_MB 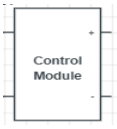	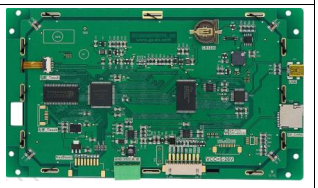

Figure 5.8: Components of pulsed power supply.

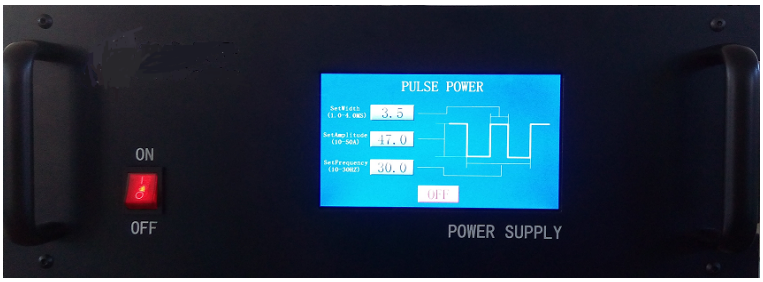

Figure 5.9: Front panel of the power supply

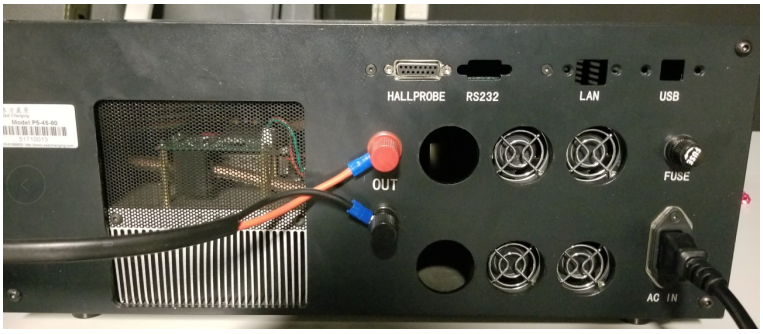

Figure 5.10: Rear panel of the power supply

(range of 1.0 to 4.0 ms), 2) the output current setting (range of 10 to 50 A), and (3) the output frequency range (10 to 30 Hz). Clicking on the corresponding button on the touch screen changes the value accordingly to determine the corrections.

The rear panel is shown in Figure 5.10. The red button is the positive pole of the current output (OUT), while the black button is the negative pole of the output. The input power outlet is connected to an AC input at 110 V.

5.3 Test

In this section, we tested the input of this electromagnet, which is also the output of the power supply, and the output of the electromagnet, which is the UPEMF waveform.

The testing process (Figure 5.9) is divided into two parts. First, we tested the output waveform of the power supply by displaying it on an oscilloscope (Figure 5.10). Second, the output waveform of the electromagnetic unit is measured by a Gauss meter.

The Hantek oscilloscope that we used is a high-performance portable oscilloscope

with a 200 MHz bandwidth and 1 GSa/s sample rate. We adjusted the waveform scale display to a size that is easy to view. The duration of signal window is set to 800 μs.

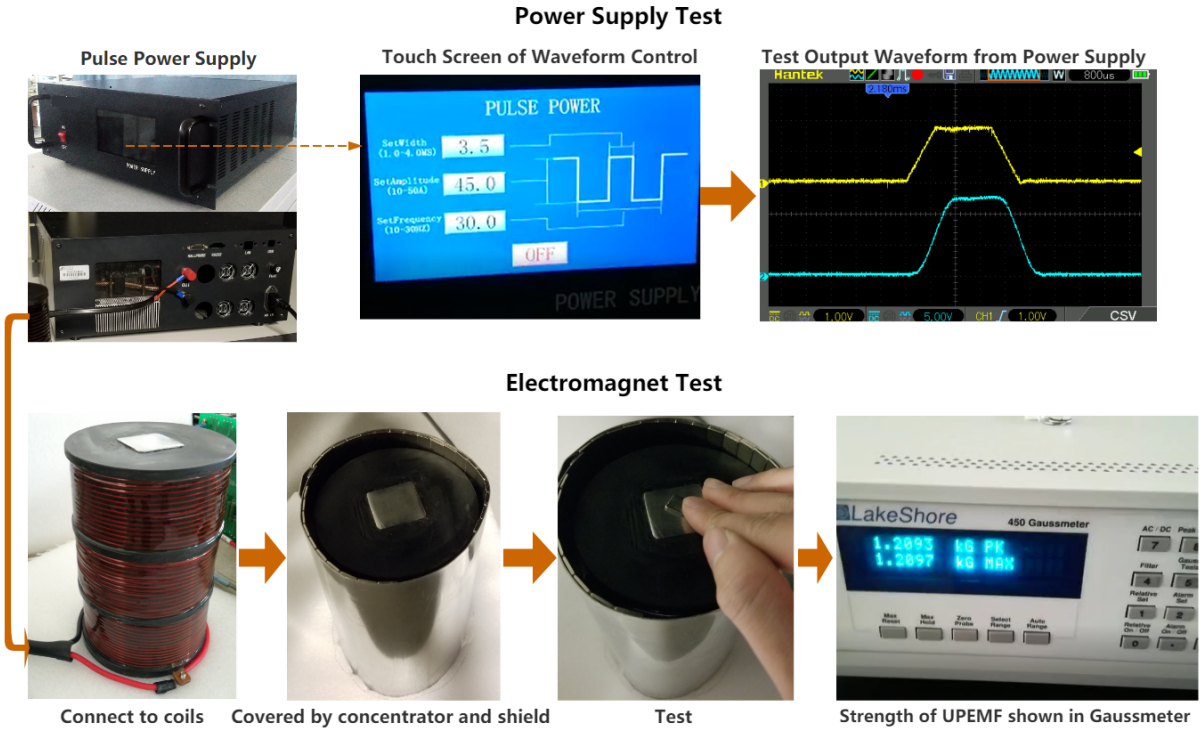

Figure 5.11: Oscilloscope settings and display.

The input of the power supply uses a triangular socket to access the 110 V 6 0Hz AC power. The connection of the positive and negative from the power supply to the electromagnet follows the *right-hand rule*. The black wire and red wire are connected firmly to the two positive and negative terminals, respectively, of the pulsed power supply, therein using an M6 insulated stud, and the electromagnet unit by a connecting piece and fixed using screws and nuts. The red terminal represents the current flowing out of the positive side, while the black terminal represents the direction of current flowing into the device.

After completing all connections, we turned on the pulse power supply and warmed up the device for a minute. Then, we used the touch screen to set the pulse width, current strength and frequency. We set the pulse width to 3.5 ms and the frequency to 30 Hz. The current is varied from 15 A to 45 A for testing. On the oscilloscope, channel 1 with

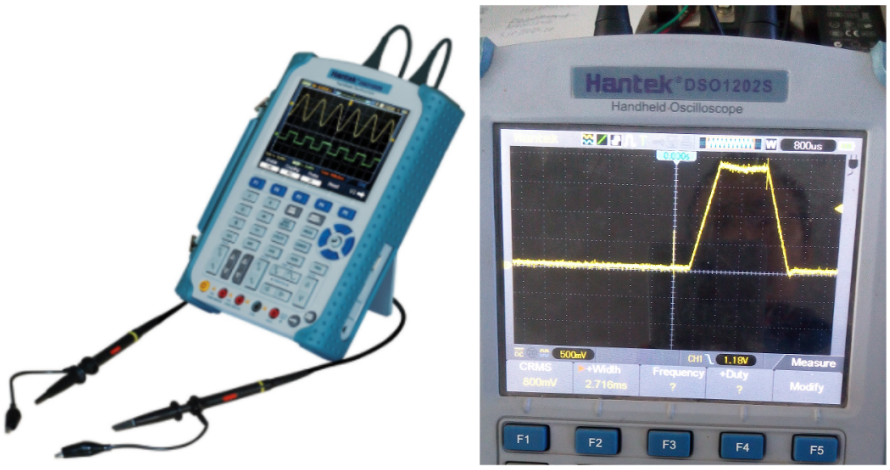

Figure 5.12: Oscilloscope settings and display.

the yellow line is the self-test of the power supply without an external load. Channel 2 displays the voltage with the load of the electromagnet. We recorded the waveform of the load through the record mode of the oscilloscope.

The change in voltage for the input current is shown in Figure 5.11. The current increases at intervals of 5 A. The left 4 charts represent the current from 10 A to 25 A, while the right 4 charts represent the current from 30 A to 45 A. The units of the voltage are set to V/100 for convenience. The duration is given by the time step. The total time step for the current is 4000, with a 3 μs step size. From the graph, we can observe the waveform shape the amplitude. Although there are some glitches in the waveform, there is no direction reversal of the current in general; therefore, we can consider this as a unipolar input pulse current. The average pulse width of the high amplitude of the current is 3.5 ms, which is measured as $(timestep2 - timestep1) \times 3\mu s$. We detected the maximum value of each input current. The 10 A current shows a maximum value of 5.2 V, and the 45 A current shows a maximum value of 18.4 V. Compared with the simulation input current in Section 4.3, Figure 4.11, the actual rectangular wave of the input current oscillates, which means that it is not a perfect rectangle. The rising time or falling time is controlled below the pulsed width time.

Given the current and voltage, we can calculate the maximum instantaneous power

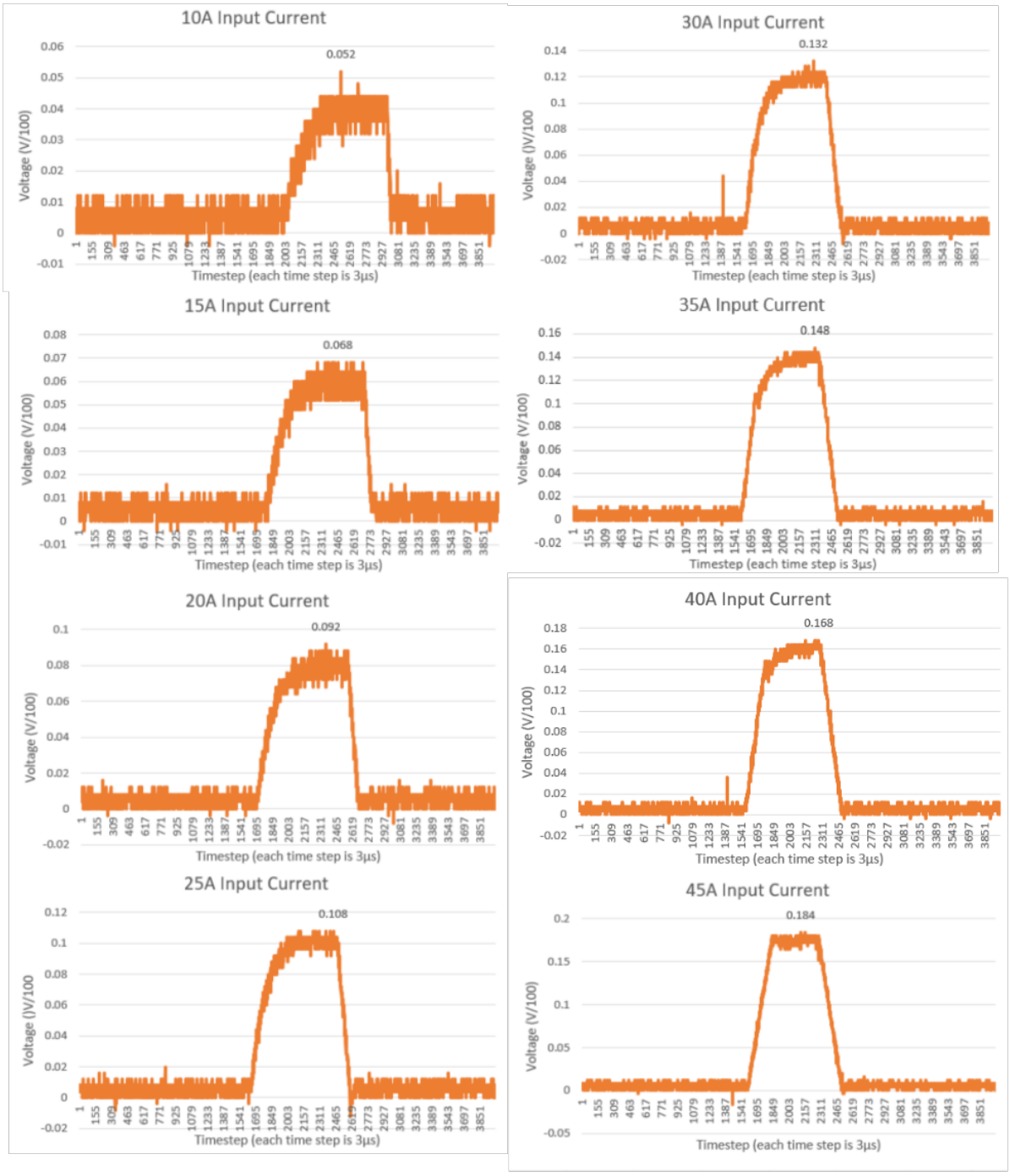

Figure 5.13: Test of input waveform.

in Figure 5.12. With increasing input current from 10 A to 45 A, the power climbs to 828 W.

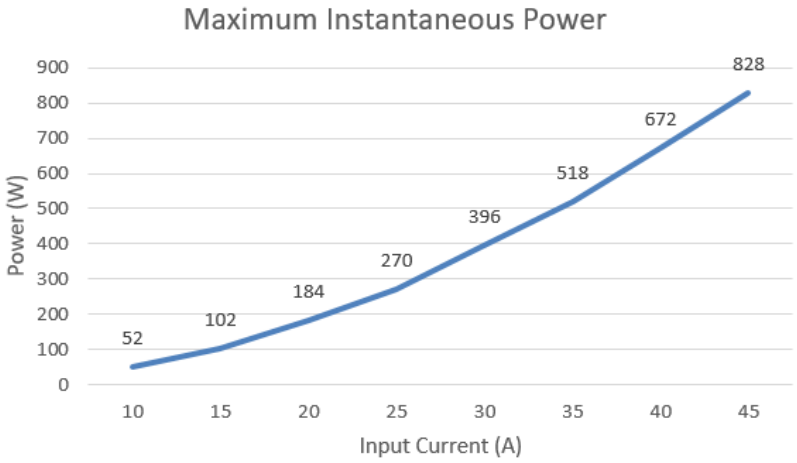

Figure 5.14: Power consumption of the UPEMF apparatus.

Second, the strength of the UPEMF is tested on the north end surface. The Gauss meter that we used in Figure 5.9 is a *LakeShore* 450, which is a high-accuracy Gauss meter for both DC and AC magnetic field measurements. Theoretically, the measurement of the magnetic field is based on the *Hall* effect. When the current is perpendicular to the external magnetic field through the conductor, the carrier is deflected, and an additional electric field is generated perpendicular to the direction of the current and the magnetic field, thereby generating a potential difference across the conductor. This phenomenon is the *Hall* effect. This potential difference is also called the *Hall* potential difference. The power probe sensor detects changes in magnetic field. The analog signal of the probe sensor is converted into digital signals. The digital signal is recorded by the internal circuitry of the Gauss meter.

When testing the magnetic field, a transverse probe is pressed onto the surface and connected to a Gauss meter. We recorded the output driven by the current from 10 A to 45 A.

The output magnetic field is shown in Figure 5.13. The intensity increased with increasing excitation current. When the electromagnet is excited by a low current, the

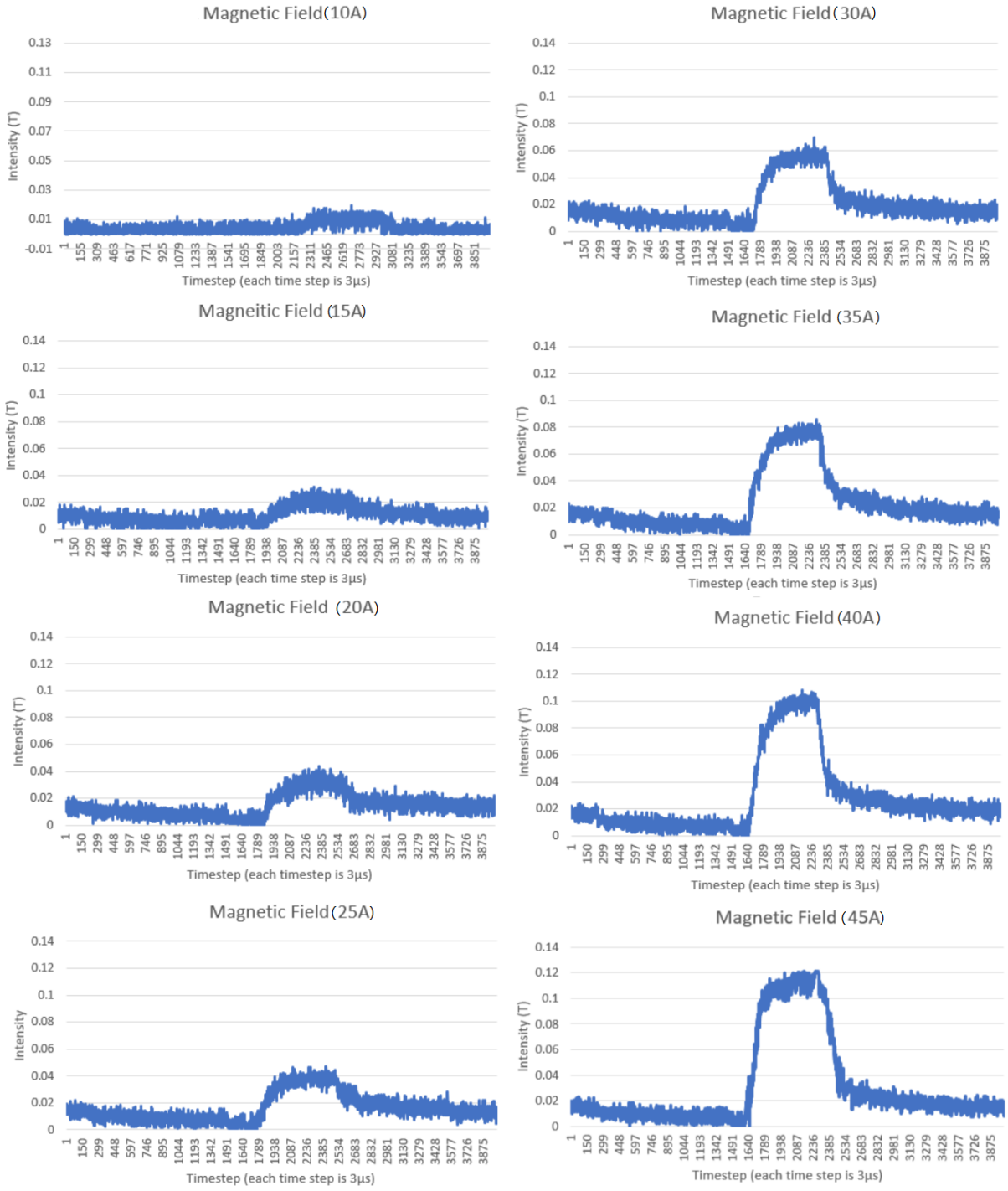

Figure 5.15: Test of the magnetic field.

peak value of the magnetic field is very low, and the rectangular shape of the magnetic field is not achieved. As the current increases, the magnetic field can gradually reach the peak value. The rectangular shape of the waveform gradually forms. However, it can be seen from the falling edge of the waveform that the magnetic field cannot decrease to zero immediately after the current decreases to zero. From the graphs for currents of 30 A to 45 A, we can roughly estimate the intensity of the remanence, which is between 0.03 T and 0.04 T. The phenomenon of remanence leads to the hysteresis effect on the waveform shape.

The maximum strength of the field reaches 1209 Gauss (0.1209 T) when the UPEMF is stable under the 45 A excitation current. On the other hand, the maximum strength of the south pole is 52 Gauss (0.0052 T). Compared to the north, the south pole is extremely weak, which means that the field can be considered to be approximately unipolar.

Compared with our simulation, the actual maximum intensity (0.12 T) of the UPEMF is less than 0.17 T. The pulse width is 3.5 ms, as desired, and the frequency of the wave is 30 Hz. When we designed and simulated the system, we added redundant value in our design in case the actual apparatus could not reach our desired intensity. The waveform trend was roughly in line with the simulation waveform. On the rising edge, the intensity climbed quickly, but after reaching a certain intensity, it could reach its peak after a short period of slow climbing. This slow climbing process was caused by the eddy current effect because the eddy currents of the shield have an obstructing effect on changes in the magnetic field. At the falling edge, similarly, the intensity first rapidly decreased to approximately 0.4 T but then subsequently experienced a slow decline process, which lasted longer than the slow climb. This is also due to the eddy current obstruction effect. In addition, the remanence in the electromagnet material also causes the magnet to maintain a certain magnetization after the excitation source decreases.

Chapter 6

Conclusions and Future Work

6.1 Conclusion

In this thesis, we designed and developed a unipolar pulse electromagnetic field apparatus, an improved medical apparatus for magnetic therapy. We introduced the concept and benefits of the UPEMF compared with the PEMF. The design requirements are determined based on literature review and discussion with medical doctor. The apparatus can potentially provide therapeutic effects such as tissue restoration. We provided an effective method of strengthening the field at the north pole and reducing the field at

the other pole using a specially designed concentrator. The differential mathematical model of the UPEMF is described for finite element modeling. We presented the results and simulations via finite element modeling for the computation of the electromagnetic field, which is driven by AC current, and the power consumption, which is caused by eddy currents. The design ideas for the pulsed power supply were discussed. We tested the output of the power supply and electromagnetic unit. This apparatus provided an approximately unipolar electromagnetic field and meets the requirements of magnetic therapy. As the apparatus has a large power with strong current (45 A), the test on patients will be performed under the professional instruction in the clinic.

6.2 Future Work

Although the first prototype of UPEMF apparatus has bee developed, numerous improvements can be achieved in the future. There are still several tasks that can be performed in further research.

- The output of the UPEMF wave should be improved. Although we have presented and developed a bio-medically usable waveform, the waveform is not perfect, as the shape is not perfectly rectangular. The density of the electromagnetic field also needs to be increased. The attenuation of the magnetic wave is violent; a stronger magnetic field can effect deep tissue in the body, achieving greater medical benefits.

- The pulsed power supply needs to be carefully designed and improved. Since the output of UPEMF is strongly related to the input current, a power supply should be specially designed. The power supply should output a certain reverse current or specific waveform to reduce or eliminate remanence in the electromagnet.

- The electromagnetic unit needs to be smaller since our electromagnetic unit will be applied to patients. Compared with PEMF devices on the market, the power supply and the electromagnet unit are too large. A portable device is easier to

operate by hand. This device is also heavy. Thus, the number of coils and the the magnetic core should be redesigned.

- The power consumption of this apparatus is high. Methods for reducing power consumption need to be considered. For safety reasons, smaller power consumptions mean smaller currents in the electromagnet.

- The bio-medical effects of our UPEMF apparatus need to be evaluated. A control test of the UPEMF should be performed by professional medical specialists. Engineers and scientist should perform long-duration research on the effects of UPEMFs on both animals and humans.

References

[1] *1DI480A-055 Datasheet*. URL: http://pdf1.alldatasheet.com/datasheet-pdf/view/107591/FUJI/1DI480A-055.html (visited on 03/26/2018).

[2] J. Novicki A. Grainys. "The Investigation of 3D Magnetic Field Distribution in Multilayer coils". In: *Electronics and Electrical Engineering* 9.12 (1988), pp. 270–273.

[3] A. Pressman. *Switching Power Supply Design*. 1998.

[4] R. Mittra AF. Peterson SL. Ray. *Computational Methods for Electromagntics*. 1998.

[5] T.W. Nehl A.M. Pawlak. "Transient Finite Element Modelling of Solenoid Actuator: The Coupled Power Electronics, Mechanical, and Magnetic Field Problem". In: *IEEE Transactions on Magnetics* 24.1 (1988), pp. 270–273.

[6] *ANSYS Maxwell*. URL: https://www.ansys.com/products/electronics/ansys-maxwell.

[7] B. S. Guru. *Electromagnetic Field Theory Fundamentals*. 1998.

[8] L. Bassett C. Andrew. "Beneficial Effects of Electromagnetic Fields". In: *Journal of Cellular Biochemistry* 51 (1997), pp. 87–393.

[9] I. Cosic D. Cvetkovic E. D. Übeyli. “Wavelet Transform Feature Extraction from Human PPG, ECG, and EEG Signal Responses to ELF PEMF Exposures: A Pilot Study”. In: *Digital Signal Processing* 18.5 (2008), pp. 861–874.

[10] D.A. Hodges. “Darlington’s Contributions to Transistor Circuit Design”. In: *IEEE Transactions on Circuits and Systems I: Fundamental Theory and Applications* 46.1 (1999), pp. 102–104.

[11] D.L. Atherton D.C. Jiles. “Theory of Ferromagnetic Hysteresis”. In: *Journal of Magnetism and Magnetic Materials* 61.2 (1986), pp. 48–60.

[12] D.Y. Chen F. Lin. “Reduction of Power Supply EMI Emission by Switching Frequency Modulation”. In: *IEEE Transactions on Power Electronics* 9.1 (1994), pp. 132–137.

[13] Y. Sun G. Bai R.W. Gao. “Study of high-coercivity sintered NdFeB magnets”. In: *Journal of Magnetism and Magnetic Materials* 308.1 (2007), pp. 20–23.

[14] A. de Hoop G. Mur. “A Finite-element Method for Computing Three-dimensional Electromagnetic Fields in Inhomogeneous Media”. In: *IEEE Transactions on Magnetics* 21.6 (1985), pp. 2188–2191.

[15] H. E. Knoepfel. “Magnetic Fields: A Comprehensive Theoretical Treatise for Practical Use”. In: *John Wiley Sons* (2008).

[16] T. Hiratani H. Haiji K. Okada. “Magnetic Properties and Workability of 6.5% Si Steel Sheet”. In: *Journal of Magnetism and Magnetic Materials* 160.1 (1996), pp. 109–114.

[17] C. Zhao H. Li Y. Yi. “Control Method and Control Circuit for Switching Power Supply”. In: *US20180054128A1* (2016).

[18] D. Pierson H. Lorenzi C. Ott. “Study of the Impact of Long-term Space Travel on the Astronauts’ Microbiome”. In: *NASA Johnson Space Center* (2017).

[19] H. Almansour H. Mohamed. "Uni-polar Pulsed Electromagnetic Medical Apparatus and Methods of Use". In: *U.S. Patent 20160228723* (2016).

[20] K. Nam H. Song. "Dual Current Control Scheme for PWM Converter under Unbalanced Input Voltage Conditions". In: *IEEE Transactions on Industrial Electronics* 46.5 (1999), pp. 953–959.

[21] B.J. McRee I.J. Cohen D.A. Weltz Jr. "Fuzzy Logic Control of a Hybrid Energy Storage Module for Use as a High Rate Prime Power Supply". In: *IEEE Transactions on Dielectrics and Electrical Insulation* 24.6 (2017), pp. 3887–3893.

[22] M. Ryu J. Kim. "High Voltage Pulse Power Supply Using Marx Generator Solid-State Switches". In: *Proceedings of the 31st Annual Conference of IEEE Industrial Electronics Society* (2005).

[23] J. Mallinson. "One-sided Fluxes - A Magnetic Curiosity". In: *IEEE Transactions on Magnetics* 9.4 (1973), pp. 678–682.

[24] X. perpina J. Milan P. Godignon. "A Survey of Wide Bandgap Power Semiconductor Devices". In: *IEEE Transactions on Power Electronics* 29.5 (2013), pp. 2155–2163.

[25] O. Bragina J. Philippides Y. Yang. "Effect of Pulsed Electromagnetic Field on the Proliferation and Differentiation Potential of Human Bone Marrow Mesenchymal Stem Cells". In: *Translational Stroke Research* 30.4 (2009), pp. 251–260.

[26] O. Bragina J. Philippides Y. Yang. "Effect of Pulsed Electromagnetic Field (PEMF) on Infarct Size and Inflammation after Cerebral Ischemia in Mice". In: *Translational Stroke Research* 5.4 (2014), pp. 491–500.

[27] S. Ano K. Sato S. Ninomiya. "Leakage Flux Effect on a Long Time-constant of Transient Eddy Current in a Solid Magnet". In: *IEEE Transactions on Applied Superconductivity* 10.1 (2000), pp. 657–660.

[28] M. Yan L.Q. Yu Y.H. Wen. "Effects of Dy and Nb on the Magnetic Properties and Corrosion Resistance of Sintered NdFeB". In: *Journal of Magnetism and Magnetic Materials* 283.3 (2004), pp. 353–356.

[29] L.R. Tejera. "Pulsed Electromagnetic Field Device". In: *Electrical Engineering Senior Design* (2014), Comillas Pontifical Universtiy.

[30] J. Sievert M. Enokizono T. Suzuki. "Rotational Power Loss of Silicon Steel Sheet". In: *IEEE Transactions on Magnetics* 26.5 (1990), pp. 2562–2564.

[31] M. Markov. "Biological Windows': A Tribute to W.Ross Adey". In: *Environmentalist* 25.4 (2005), pp. 67–74.

[32] M. S. Markov. "Expanding Use of Pulsed Electromagnetic Field Therapies". In: *Electromagnetic Biology and Medicine* 26 (2007), pp. 257–274.

[33] I. Mayergoyz. "Mathematical Models of Hysteresis". In: *IEEE Transactions on Magnetics* 22.5 (1986), pp. 603–608.

[34] J.L. Shupack M.J.Stiller G. H. Pak. "A Portable Pulsed Electromagnetic Field (PEMF) Device to Enhance Healing of Recalcitrant Venous Ulcers: A Double-blind, Placebo-controlled Clinical Trial". In: *British Journal of Dermatology* 127.2 (1992), pp. 147–154.

[35] Mojtaba Karbalayi Mohamad Reza Bayatiani Fatemeh Seif. "Design and Fabrication of a Magneitc Field Generator with Variable Intensity and Frequency for use in Medical and Biological Studies". In: *Bioelectromagnetics* 1.1 (2015), pp. 1–5.

[36] A. W. Thomas N. M. Shupak F. S. Prato. "Therapeutic Uses of Pulsed Magnetic-field Exposure: A Review". In: *Electromagnetic Biology and Medicine* 2003.307 (2003), pp. 9–32.

[37] K. Soejima P. Diniz K. Shomura. "Effects of Pulsed Electromagnetic Field (PEMF) Stimulation on Bone Tissue Like Formation are Dependent on the Maturation Stages of the Osteoblasts". In: *Bioelectromagnetics* 23.5 (2002), pp. 398–405.

[38] P. Sittiprapaporn P. Liwluck. “Effect of Pulse Electromagnetic Field Therapy to Brainwave on the Quantum Resonance System”. In: *Proceeding on ICDAMT* (2017).

[39] P. Sankar. “Magnetic arrays with increased magnetic flux”. In: *US Patent 8,514,047* (2013).

[40] V.N. Kbore P.G. Park W.S. Kim. “Generation of Uniform Magnetic Field Using a Single-layer Solenoid with multi-current method”. In: *Journal of Metrology Society of India* 24.1 (2008), pp. 9–14.

[41] A. Saddik Q. Zhang H. Dong. “Magnetic Field Control for Haptic Display: System Design and Simulation”. In: *IEEE Access* 4 (2015).

[42] R. Araneo S. Celozzi G. Lovat. “Electromagnetic shielding”. In: *New York, NY USA: Wiley* (2008).

[43] Marko S. Markov. “Pulsed Electromagnetic Field Therapy History, State of the Art and Future”. In: *Environmentialist* 27.4 (2007), pp. 465–475.

[44] T. Goodwin. “Physiological and Molecular Genetic Effects of Time-varying Electromagnetic Fields on Human Neuronal Cells”. In: *Tech. Rep. NASA/TP-2003-212054* (2003).

[45] C. Parker T. Goodwin. “Apparatus and Method for Enhancing Tissue Repair in Mammals”. In: *U.S. Patent 7601114* (2009).

[46] S. Sano Y. Kawase T. Yamaguchi. “3-D Eddy Current Analysis in a Silicon steel Sheet of an Interior Permanent Magnet Motor”. In: *IEEE Transactions on Magnetics* 39.3 (2003), pp. 1448–1451.

[47] C. Yon-Do Y. Sang-Baeck H. Jin. “Shape Optimization of Solenoid Actuator Using Finite Element Method and Numerical Optimization Technique”. In: *IEEE Transactions on Magnetics* 33 (1997), pp. 4140–4142.

[48] S. Masuda Y. Takada M. Abe. “Commercial Scale Production of Fe-6.5 wt.% Si Sheet and its Magnetic Properties”. In: *Journal of Applied Physics* 64.10 (1998).